Atmos. Meas. Tech. Discuss., https://doi.org/10.5194/amt-2018-235
Manuscript under review for journal Atmos. Meas. Tech.
Discussion started: 6 August 2018

Atmospheric Measurement Techniques Discussions

An Improved Total and Tropospheric NO_2 Column Retrieval for GOME-2

Song Liu[1], Pieter Valks[1], Gaia Pinardi[2], Isabelle De Smedt[2], Huan Yu[2], Steffen Beirle[3], and Andreas Richter[4]

[1]Deutsches Zentrum für Luft- und Raumfahrt (DLR), Institut für Methodik der Fernerkundung (IMF), Oberpfaffenhofen, Germany
[2]Belgian Institute for Space Aeronomy (BIRA-IASB), Brussels, Belgium
[3]Max Planck Institute for Chemistry, Mainz, Germany
[4]Institute of Environmental Physics (IUP-UB), University of Bremen, Bremen, Germany

Correspondence to: Song Liu (Song.Liu@dlr.de)

Abstract. An improved algorithm for the retrieval of total and tropospheric nitrogen dioxide (NO_2) columns from the Global Ozone Monitoring Experiment-2 (GOME-2) is presented. The refined retrieval will be implemented in a future version of the GOME Data Processor (GDP) as used by the EUMETSAT Satellite Application Facility on Atmospheric Composition and UV Radiation (AC-SAF). The first main improvement is the application of an extended 425-497 nm wavelength fitting window in the differential optical absorption spectroscopy (DOAS) retrieval of the NO_2 slant column density. Updated absorption cross-sections and a linear offset correction are used for the large fitting window. An improved slit function treatment is applied to compensate for both long-term and in-orbit drift of the GOME-2 slit function. Compared to the current operational (GDP 4.8) dataset, the use of these new features increases the NO_2 columns by $\sim$1-3 $\times$ 10^{14} molec/cm^2 and reduces the slant column error by $\sim$24%. In addition, the bias between GOME-2A and GOME-2B measurements is largely reduced by adopting a new level 1b data version in the DOAS retrieval. The retrieved NO_2 slant columns show good consistency with the Quality Assurance for Essential Climate Variables (QA4ECV) retrieval with a good overall quality. Second, the STRatospheric Estimation Algorithm from Mainz (STREAM), which was originally developed for the TROPOspheric Monitoring Instrument (TROPOMI) instrument, was optimized for GOME-2 measurements to determine the stratospheric NO_2 column density. Applied to synthetic GOME-2 data, the estimated stratospheric NO_2 columns from STREAM shows a good agreement with the a priori truth. An improved latitudinal correction is introduced in STREAM to reduce the biases over the subtropics. Applied to GOME-2 measurements, STREAM largely reduces the overestimation of stratospheric NO_2 columns over polluted regions in the GDP 4.8 dataset. Third, the calculation of AMF applies an updated box-air mass factor (box-AMF) look-up table (LUT) calculated using the latest version of VLIDORT model with an increased number of reference points and vertical layers, a new GOME-2 surface albedo climatology, improved a priori NO_2 profiles obtained from the TM5-MP chemistry transport model, and improved GOME-2 cloud parameters. A large effect on the retrieved tropospheric NO_2 columns (more than 10%) is found over polluted regions. To evaluate the GOME-2 tropospheric NO_2 columns, an end-to-end validation is performed using ground-based multiple-axis DOAS (MAXDOAS) measurements. The validation is illustrated for 6 stations covering urban,

Atmos. Meas. Tech. Discuss., https://doi.org/10.5194/amt-2018-235
Manuscript under review for journal Atmos. Meas. Tech.
Discussion started: 6 August 2018

Atmospheric Measurement Techniques Discussions

suburban, and background situations. Compared to the GDP 4.8 product, the new dataset presents an improved agreement with the MAXDOAS measurements for all the stations.

1 Introduction

Nitrogen dioxide (NO_2) is an important trace gas in the Earth's atmosphere. In the stratosphere, NO_2 is strongly related to halogen compound reactions and ozone destruction (Solomon, 1999). In the troposphere, nitrogen oxides (NO_x=NO_2+NO) serve as a precursor of ozone and secondary aerosol in the presence of volatile organic compounds (VOC) (Seinfeld et al., 1998). As a prominent air pollutant affecting human health and ecosystem, large amounts of NO_2 are produced in the boundary layer by industrial processes, power generation, transportation, and biomass burning over polluted hot spots. For instance, a strong growth of NO_2 since two decades has caused severe air pollution problems for China with largest NO_2 columns in 2011, since then, cleaner techniques and stricter controlling have been applied to reduce the NO_2 pollution (Richter et al., 2005; Mijling et al., 2017; Liu et al., 2017). An increase in NO_2 concentrations due to economic growth is also found over India with a peak in 2012 (Hilboll et al., 2017). Despite the decrease in NO_x emissions in Europe, still around half of European Union member states exceed the air quality standards mainly caused by diesel car emissions (European Commission, 2017).

NO_2 column measurements have been provided by satellite instruments, e.g., Global Ozone Monitoring Experiment (GOME) (Burrows et al., 1999), SCanning Imaging Absorption SpectroMeter for Atmospheric CHartographY (SCIAMACHY) (Bovensmann et al., 1999), Ozone Monitoring Instrument (OMI) (Levelt et al., 2006), and Global Ozone Monitoring Experiment-2 (GOME-2) (Callies et al., 2000; Munro et al., 2016). NO_2 observations will be continued by the new generation instruments with high spatial resolution such as TROPOspheric Monitoring Instrument (TROPOMI) (launched in October 2017, Veefkind et al., 2012) and by geostationary missions such as Sentinel-4 (Ingmann et al., 2012). The GOME-2 instrument, which is the main focus of this study, is included on a series of MetOp satellites as part of the EUMETSAT Polar System (EPS). The first GOME-2 was launched in October 2006 aboard the MetOp-A satellite, and a second GOME-2 was launched in September 2012 aboard MetOp-B. The consistent long-term dataset will be further extended by the third GOME-2 on the upcoming MetOp-C platform (to be launched in September 2018). NO_2 measurements from GOME-2 have been widely used to characterise the distribution, evolution, or transport of NO_2 (e.g., Hilboll et al., 2013, 2017; Zien et al., 2014), to estimate the NO_x emission (e.g., Gu et al., 2014; Miyazaki et al., 2017; Ding et al., 2017), and to interpret VOC levels, ozone variation, or anthropogenic aerosol loading (e.g., Vrekoussis et al., 2010; Safieddine et al., 2013; Penning de Vries et al., 2015).

The GOME-2 total and tropospheric NO_2 products are generated using the GOME Data Processor (GDP) algorithm at the German Aerospace Center (DLR). The retrieval algorithm has been first described by Valks et al. (2011) as implemented in the GDP version 4.4 and was later updated to the current operational version 4.8 (Valks et al., 2017). The NO_2 retrieval for GOME-2 follows a classical 3-steps scheme. (1) The total NO_2 slant columns (namely the concentration integrated along the effective light path from the Sun through the atmosphere to the instrument) are derived using the differential optical absorption spectroscopy (DOAS) method (Platt and Stutz, 2008). The DOAS technique is a least-squares method fitting the molecular absorption cross-sections to the measured GOME-2 (ir)radiances provided by the EUMETSAT's processing facility.

Atmos. Meas. Tech. Discuss., https://doi.org/10.5194/amt-2018-235
Manuscript under review for journal Atmos. Meas. Tech.
Discussion started: 6 August 2018

Atmospheric Measurement Techniques Discussions

The fit is applied on the data within a fitting window optimized for NO_2. As analysed by Richter et al. (2011) and in the Quality Assurance for Essential Climate Variables (QA4ECV, www.qa4ecv.eu) project, extension of the fitting window for GOME-2 increases the signal-to-noise ratio and hence improves the NO_2 slant column error. (2) The stratospheric contribution is estimated and separated from the NO_2 slant columns (referred to as stratosphere-troposphere separation). The GDP 4.8 algorithm applies a modified reference sector method, which uses measurements over clean regions to estimate the stratospheric NO_2 columns based on the assumption of longitudinally invariable stratospheric NO_2 layers and of negligible tropospheric NO_2 abundance over the clean areas. The modified reference sector method defines a global pollution mask to remove potentially polluted regions and applies an interpolation over the unmask areas to derive the stratospheric NO_2 columns. As a result of using a fixed pollution mask, the modified reference sector method in GDP 4.8 has larger uncertainties over polluted areas, because limited amount of information over continents is used. To overcome the shortcomings, the STRatospheric Estimation Algorithm from Mainz (STREAM) method (Beirle et al., 2016) has been developed for TROPOMI instrument and was also successfully applied on GOME, SCIAMACHY, OMI, and GOME-2 measurements. Belonging also to the modified reference sector method, STREAM defines not a fixed pollution mask but weighting factors for each observation to determine its contribution to the stratospheric estimation. (3) The tropospheric NO_2 vertical columns are calculated from the tropospheric slant columns by an air mass factor (AMF) calculation, which contributes the largest uncertainty to the NO_2 retrieval, in particular over polluted regions (Boersma et al., 2004). The AMFs are determined with a radiative transfer model (RTM) requiring ancillary information like surface parameters, vertical shape of the a priori NO_2 profile, and cloud information.

In this paper, a new algorithm to retrieve the total and tropospheric NO_2 for the GOME-2 instruments is described which includes improvements in each of the 3 algorithm steps introduced above. The improved algorithm will be implemented in the next version of GDP (referred to as GDP 4.9 hereafter). We briefly introduce the GOME-2 instrument (Sect. 2) and the current operational (GDP 4.8) total and tropospheric NO_2 retrieval algorithm (Sect. 3). We present the improvements to the DOAS slant column retrieval (Sect. 4), the stratosphere-troposphere separation (Sect. 5), and the AMF calculation (Sect. 6). Finally, we show an end-to-end validation of the tropospheric NO_2 dataset using ground-based multiple-axis DOAS (MAXDOAS) datasets with different pollution conditions (Sect. 7).

2 Instrument and measurements

GOME-2 is a nadir-scanning UV-VIS spectrometer aboard the MetOp-A and MetOp-B satellites (referred to as GOME-2A and GOME-2B throughout this study) with a satellite repeating cycle of 29 days and an equator crossing time of 9:30 local time (descending node). The GOME-2 instrument measures the Earth's backscattered radiance and extra-terrestrial solar irradiance in the spectral range between 240 and 790 nm. The morning measurements from GOME-2 provide a better understanding of the diurnal variations of the NO_2 columns in combination with afternoon observations from for example the OMI and TROPOMI instruments (13:30 local time). The default swath width of GOME-2 is 1920 km, enabling a global coverage in $\sim$1.5 days. The default ground pixel size is 80×40 km^2 in the forward scan, which remains almost constant over the full swath width. In a tandem operation of MetOp-A and MetOp-B from July 2013 onwards, a decreased swath of 960 km and an increased spatial

Atmos. Meas. Tech. Discuss., https://doi.org/10.5194/amt-2018-235
Manuscript under review for journal Atmos. Meas. Tech.
Discussion started: 6 August 2018

Atmospheric Measurement Techniques Discussions

resolution of 40×40 km^2 are employed by GOME-2A. See Munro et al. (2016) for more details on instrument design and performance.

The operational GOME-2 NO_2 product is provided by DLR in the framework of EUMETSAT's Satellite Application Facility on Atmospheric Composition Monitoring (AC-SAF). The product processing chain starts with the level 0 to 1b processing within the core ground segment at EUMETSAT in Darmstadt (Germany), where the raw instrument (level 0) data is converted into geolocated and calibrated (level 1b) (ir)radiances by the GOME-2 Product Processing Facility (PPF). The level 1b (ir)radiances are disseminated through the EUMETCast system to the AC-SAF processing facility at DLR in Oberpfaffenhofen (Germany), and further processed using the Universal Processor for UV/VIS Atmospheric Spectrometers (UPAS) system. Broadcasted via EUMETCast, WMO/GTS, and the Internet, the resulting level 2 near-real-time total column products including NO_2 columns can be received by user communities 2 hours after sensing. Offline and reprocessed GOME-2 level 2 and consolidated products are also provided within 1 day by DLR, which can be ordered via FTP-server and the EUMETSAT Data Centre (https://acsaf.org/).

3 Total and tropospheric NO_2 retrieval

The first main step of the retrieval algorithm is the DOAS technique, which is applied to determine the total NO_2 slant columns from the (ir)radiance spectra measured by the instrument. Based on the Beer-Lambert's law, the DOAS fit is a least-squares inversion to isolate the trace gas absorption from the background processes, e.g., extinction resulting from scattering on molecules and aerosols, with a background polynomial $P(\lambda)$ at wavelength λ:

$$\ln\left[\frac{I(\lambda)+offset(\lambda)}{I^0(\lambda)}\right] = -\sum_g S_g\sigma_g(\lambda) - \alpha_R R(\lambda) - P(\lambda). \quad (1)$$

The measurement-based term is defined as the natural logarithm of the measured earthshine radiance spectrum $I(\lambda)$ with a constant intensity offset correction $offset(\lambda)$ divided by the daily solar irradiance spectrum $I^0(\lambda)$. The spectral effect from the absorption of species g is determined by the fitted slant column density S_g and associated absorption cross-section $\sigma_g(\lambda)$. An additional term with the Ring scaling factor α_R and the Ring reference spectrum $R(\lambda)$ describes the filling-in effect of Fraunhofer lines by rotational Raman scattering (the so-called Ring effect). The GDP 4.8 algorithm adopts a wavelength range of 425-450 nm to ensure prominent NO_2 absorption structures and controllable interferences from other absorbing species, e.g., water vapor (H_2O_{vap}), ozone (O_3), and oxygen dimer (O_4). Table 1 gives an overview of the DOAS settings for the current operational GDP 4.8 algorithm, the improved version 4.9 algorithm (see Sect. 4), and the algorithm used in the QA4ECV product (see Sect. 4.5).

The second component in the retrieval is the calculation of initial total vertical column densities V_{init} using an stratospheric AMF (M_{strat}) conversion:

$$V_{init} = \frac{S}{M_{strat}}. \quad (2)$$

Atmos. Meas. Tech. Discuss., https://doi.org/10.5194/amt-2018-235
Manuscript under review for journal Atmos. Meas. Tech.
Discussion started: 6 August 2018

Atmospheric Measurement Techniques Discussions

Table 1. Main settings of GOME-2 DOAS retrieval of NO_2 slant columns discussed in this study.

	GDP 4.8 (Valks et al., 2011, 2017)	GDP 4.9 (this work)	QA4ECV (Müller et al., 2016; Boersma et al., 2018)
Wavelength range	425-450 nm	425-497 nm	405-465 nm
Cross-sections	NO_2 240K, H_2O_{vap}, O_3, O_4, Ring	NO_2 220K, H_2O_{vap}, O_3, O_4, Ring, H_2O_{liq}, Eta, Zeta, resol correction	NO_2 220K, H_2O_{vap}, O_3, O_4, Ring, H_2O_{liq}
Polynomial degree	3	5	5
Intensity offset	Constant ($ln(I+a)$)	Linear ($ln(I+a+b\lambda)$)	Constant ($ln(I^0)+a/I^0$)
Slit function	Preflight	Stretched preflight	Preflight

Given the small optical thickness of NO_2, M_{strat} can be determined as:

$$M_{strat} = \frac{\sum_l m_l(\boldsymbol{b}) x_l c_l}{\sum_l x_l} \tag{3}$$

with m_l the box-air mass factors (box-AMFs) in layer l, x_l the altitude-dependent subcolumns from a stratospheric a priori NO_2 profiles climatology (Lambert et al., 1999), and c_l a correction coefficient to account for the temperature dependence of NO_2 cross-section (Boersma et al., 2004; Nüß et al., 2006). The calculation of V_{init} assumes negligible tropospheric NO_2 and hence uses only the stratospheric a priori NO_2 profiles to derive AMF. The box-AMFs m_l are derived using the multi-layered multiple scattering LIDORT RTM (Spurr et al., 2001) and stored in a look-up table (LUT) as a function of various model inputs $\boldsymbol{b}$, including GOME-2 viewing geometry, surface pressure, and surface albedo. The surface albedo is described by the Lambertian-equivalent reflectivity (LER). The surface LER climatology used in the GDP 4.8 algorithm is derived from combined TOMS/GOME measurements (Boersma et al., 2004) for the years 1979-1993 with a spatial resolution of 1.25°lon×1.0°lat.

In the presence of clouds, the calculation of M_{strat} adopts the independent pixel approximation based on GOME-2 cloud parameters:

$$M_{strat} = \omega M_{strat}^{cloud} + (1-\omega) M_{strat}^{clear} \tag{4}$$

with ω the cloud radiance fraction, M_{strat}^{cloud} the cloudy-sky stratospheric AMF, and M_{strat}^{clear} the clear-sky stratospheric AMF. M_{strat}^{cloud} and M_{strat}^{clear} are derived with Eq. (3) with M_{strat}^{cloud} mainly relying on the cloud pressure and the cloud albedo. ω is derived from the cloud fraction c_f:

$$\omega = \frac{c_f I^{cloud}}{(1-c_f) I^{clear} + c_f I^{cloud}}, \tag{5}$$

where I^{cloud} is the radiance for a cloudy scene and I^{clear} for a clear scene. I^{cloud} and I^{clear} are calculated using LIDORT, depending mostly on the GOME-2 viewing geometry, surface albedo and cloud albedo. From GOME-2, c_f is determined with the Optical Cloud Recognition Algorithm (OCRA), and the cloud pressure and the cloud albedo are derived using the Retrieval Of Cloud Information using Neural Networks (ROCINN) algorithm (Loyola et al., 2007, 2011).

Atmos. Meas. Tech. Discuss., https://doi.org/10.5194/amt-2018-235
Manuscript under review for journal Atmos. Meas. Tech.
Discussion started: 6 August 2018

Atmospheric Measurement Techniques Discussions

The next retrieval step is the separation of stratospheric and tropospheric components from the initial vertical total columns, namely the "stratosphere-troposphere separation". Since no direct stratospheric measurements are available for GOME-2, a spatial filtering algorithm is applied to estimate the stratospheric NO_2 columns in GDP 4.8. The spatial filtering algorithm belongs to the modified reference sector method, which uses total NO_2 columns over clean regions to approximate the stratospheric NO_2 columns based on the assumption of longitudinally invariable stratospheric NO_2 layers and of negligible tropospheric NO_2 abundance over the clean areas. The spatial filtering algorithm uses a pollution mask to filter the potentially polluted areas (tropospheric NO_2 columns larger than 1×10^{15} molec/cm^2), followed by a low-pass filtering (with a zonal 30°boxcar filter) on the initial total columns of the unmasked areas, and afterwards a removal of a tropospheric background NO_2 (1×10^{14} molec/cm^2) from the derived stratospheric columns.

Finally, the tropospheric NO_2 columns V_{trop} can be computed as:

$$V_{trop} = \frac{M_{strat}}{M_{trop}} \times T, \tag{6}$$

where M_{strat} is the stratospheric AMF in Eq. (3), M_{trop} is the tropospheric AMF, and T is the tropospheric residues ($T = V_{init} - V_{strat}$). M_{trop} is determined using Eq. (3) and (4) with tropospheric a priori NO_2 profiles. The calculation of M_{trop} relies on the same model parameters as of M_{strat}, but the dependency on the parameters like surface albedo and cloud properties as well as on the a priori NO_2 profiles is much stronger. The GDP 4.8 adopts the tropospheric a priori NO_2 profiles from a run of global chemistry transport model MOZART version 2 (Horowitz et al., 2003) with anthropogenic emissions from the EDGAR2.0 inventory (Olivier et al., 1996) for the early 1990s. The monthly average vertical profiles are calculated from MOZART-2 data from the year 1997 for the overpass time of GOME-2 (9:30 local time) with a resolution of 1.875°lon×1.875°lat.

4 Improved DOAS slant column retrieval

A larger 425-497 nm wavelength fitting window for the DOAS method (Richter et al., 2011) is implemented in the GDP 4.9 to retrieve the NO_2 slant columns, which improves the signal-to-noise ratio by including more NO_2 absorption structures. Compared to the extended 405-465 nm range, as employed by the QA4ECV GOME-2 NO_2 product and used in the NO_2 retrieval for OMI instrument (Boersma et al., 2002; van Geffen et al., 2015), the 425-497 nm fitting window has stronger sensitivity to NO_2 columns in boundary layer because the importance of scattering decreases with wavelength (Richter and verification team, 2015). In this study, the slant columns are derived using QDOAS software developed at the Belgian Institute for Space Aeronomy (BIRA-IASB) (Danckaert et al., 2015) [1]. Table 1 summarises the new settings of the GDP 4.9 algorithm.

[1]Note that the derived slant columns are scaled by geometric AMFs to correct for the angular dependencies of GOME-2 measurements in this section.

Atmos. Meas. Tech. Discuss., https://doi.org/10.5194/amt-2018-235
Manuscript under review for journal Atmos. Meas. Tech.
Discussion started: 6 August 2018

4.1 Absorption cross-sections

In the fitting window optimized for NO_2 retrieval, the DOAS fit includes species with strong and unique absorption structures and describes their spectral effect using absorption cross-sections from literature. In our GDP 4.9 algorithm, the absorption cross-sections of NO_2, H_2O_{vap}, O_3, and O_4 are updated mainly with newly released datasets as:

- NO_2 absorption at 220K from Vandaele et al. (2002)
- O_3 absorption at 228K from Brion et al. (1998)
- H_2O_{vap} absorption at 293K from HITEMP Rothman et al. (2010), rescaled as in Lampel et al. (2015)
- O_4 absorption at 293K from Thalman and Volkamer (2013)

In addition, to compensate for the larger spectral interference from liquid water (H_2O_{liq}), a H_2O_{liq} absorption (Pope and Fry, 1997) is included to reduce systematic errors above ocean for the wider wavelength range. Two additional GOME-2 polarization key data (EUMETSAT, 2009) are included to correct for remaining polarization correction problems, particularly for GOME-2B.

- H_2O_{liq} absorption at 297K from Pope and Fry (1997), smoothed as in Peters et al. (2014)
- Eta and Zeta from GOME-2 calibration key data (EUMETSAT, 2009)

It is worth noting that our improved DOAS retrieval in the GDP 4.9 adopts a decreased temperature of NO_2 cross-section (220K instead of 240K in GDP 4.8, Valks et al. 2017) for a consistency with other NO_2 retrievals from GOME-2, OMI and TROPOMI (Müller et al., 2016; Boersma et al., 2002; van Geffen et al., 2015, 2016), with minor effect on the fit quality ($\sim$0.02%) from the two temperatures. Changing the temperature of NO_2 cross-section from 240K to 220K reduces the NO_2 slant columns by $\sim$6%-9%, but this temperature dependence is corrected in the AMF and vertical column calculation (see Eq. (3)).

The spectral signature of sand absorption has been investigated by Richter et al. (2011) for GOME-2 data, but it is not applied here because of the potential interference with the broadband liquid water structure (Peters et al., 2014), which might lead to non-physical results over the ocean.

4.2 Intensity offset correction

Besides the radiances backscattered by the Earth's atmosphere, a number of both natural (i.e. the Ring effect) and instrumental (e.g., stray light in the spectrometer and change of detector's dark current) sources contribute to an additional "offset" to the scattering intensity. To correct for this drift, an offset correction parameter is included in the DOAS fit (see Eq. (1)). Figure 1 illustrates the effect of using a intensity offset correction with a linear wavelength dependency on our NO_2 retrieval for the large fitting window on 3 March 2008. The use of a linear offset correction increases the NO_2 columns by up to 3×10^{14} molec/cm^2 (17%) and decreases the fitting residues (retrieval root-mean-square, RMS) by up to 30%. Larger differences are found at the

Atmos. Meas. Tech. Discuss., https://doi.org/10.5194/amt-2018-235
Manuscript under review for journal Atmos. Meas. Tech.
Discussion started: 6 August 2018

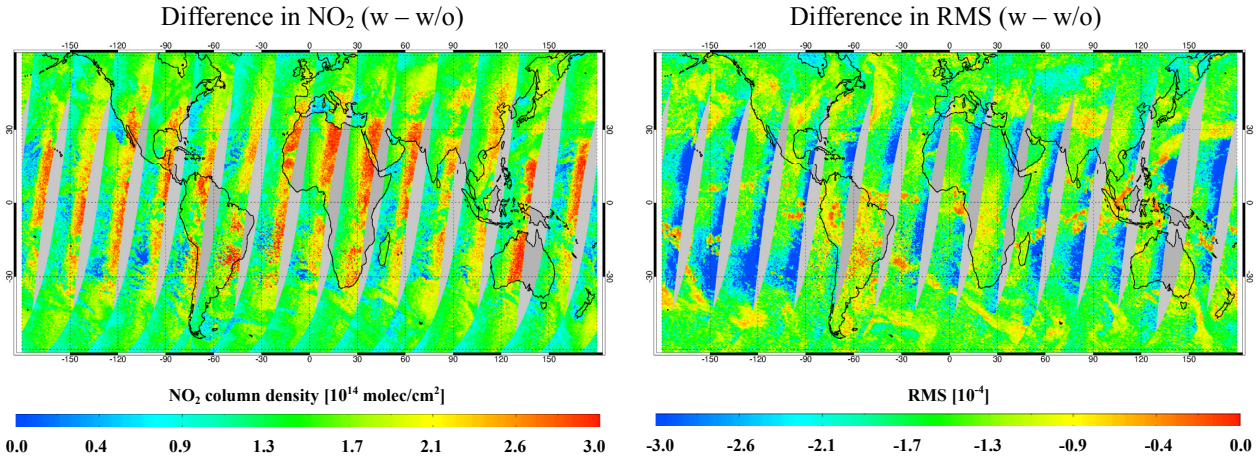

Figure 1. Difference in NO_2 columns (slant columns scaled by geometric AMFs) (left) and retrieval RMS (right) estimated with and without a linear intensity offset correction for GOME-2A on 3 March 2008.

eastern scans (eastern part of GOME-2 swath), possibly suggesting instrumental issues specific to GOME-2. For the retrieval RMS, stronger improvements are mainly located above ocean, arguably from the compensation of inelastic vibrational Raman scattering in water bodies (Vountas et al., 2003).

The intensity offset can also be fitted using only the constant term, as employed by the GDP 4.8 algorithm (with 425-450 nm wavelength window) and as recommended by the QA4ECV algorithm (with 405-465 nm). Compared to the use of linear intensity offset correction, the application of a constant term on our retrieval shows a decrease in the NO_2 columns by up to 3.5×10^{14} molec/cm^2 (17%) and an increase in the retrieval RMS by up to 14%, which implies the necessity of using a linear intensity offset correction for the large 425-497 nm wavelength range.

4.3 GOME-2 slit function treatment

An accurate treatment of the instrumental slit function is essential for the wavelength calibration and the convolution of high-resolution laboratory cross-sections. In spite of a generally good spectral stability of GOME-2 in orbit, the width of GOME-2 slit function has been changing on both long and short timescales (Munro et al., 2016), which needs to be accounted for in the DOAS analysis. In this study, an improved treatment of GOME-2 slit function in the DOAS fit is achieved by calculating effective slit functions from GOME-2 irradiance measurements to correct for the long-term variations (see Sect. 4.3.1) and by including an additional cross-section in the DOAS fit to correct for the short-term variations (see Sect. 4.3.2).

4.3.1 Long-term variations

To analyse the long-term variations of the GOME-2 instrumental slit function and the impact on our retrieval, effective slit functions are derived by convolving a high-resolution reference solar spectrum (Chance and Kurucz, 2010) with a stretched

Atmos. Meas. Tech. Discuss., https://doi.org/10.5194/amt-2018-235
Manuscript under review for journal Atmos. Meas. Tech.
Discussion started: 6 August 2018

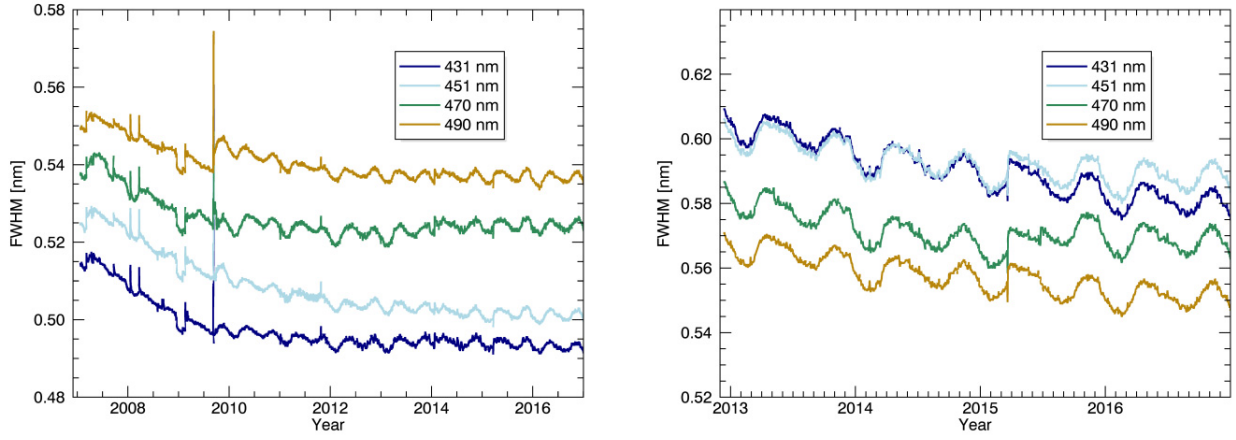

Figure 2. Temporal evolution of the fitted slit function FWHM for GOME-2A (left, January 2007-December 2016) and GOME-2B (right, December 2012-December 2016.)

preflight GOME-2 slit function and aligning to the GOME-2 daily irradiance measurements with stretch factors as fit parameters. The effective slit functions are calculated in 13 subwindows covering the full fitting window (425-497 nm). Figure 2 displays the long-term evolution of the fitted GOME-2 slit function width (full width at half maximum, FWHM) calculated from the stretch factors. The GOME-2 slit function has narrowed after the launch by ∼5% for GOME-2A and ∼3.5% for GOME-2B at 451 nm, in agreement with Dikty et al. (2011), Azam et al. (2015), and Munro et al. (2016). For GOME-2A, visible discontinuities of the slit function width are related to the in-orbit instrument operations, including an apparent anomaly in September 2009 when a major throughput test was performed (EUMETSAT, 2012). After the throughput test, the narrowing of slit function has slowed down. For GOME-2B, stronger seasonal fluctuations of the FWHM are found. The seasonal and long-term variations in the GOME-2 slit function are caused by changing temperatures of the optical bench due to the seasonal variation in solar heating and the lack of thermal stability of the optical bench, respectively (Munro et al., 2016). Although the variations are only a few percent, the effect on the DOAS retrieval is significant. Compared to the application of the preflight slit function, the use of a stretched slit function improves the calibration residuals by ∼40% for both GOME-2A and GOME-2B (not shown).

In previous studies, slit functions have also been fitted using various Gaussian shapes. For instance, De Smedt et al. (2012) have derived effective GOME-2 slit functions for formaldehyde retrieval using an asymmetric Gaussian with it's width and shape as fit parameters. For NO_2 retrieval, the use of effective slit functions with an asymmetric Gaussian leads to similar results as using a preflight slit function. In addition, Beirle et al. (2017) have proposed a slit function parameterization using a Super Gaussian, which is proved to quickly and robustly describe the slit function changes for satellite instrument OMI or TROPOMI. In the case of GOME-2, the Super Gaussian obtains nearly identical results as the asymmetric Gaussian and is therefore not applied in here.

Atmos. Meas. Tech. Discuss., https://doi.org/10.5194/amt-2018-235
Manuscript under review for journal Atmos. Meas. Tech.
Discussion started: 6 August 2018

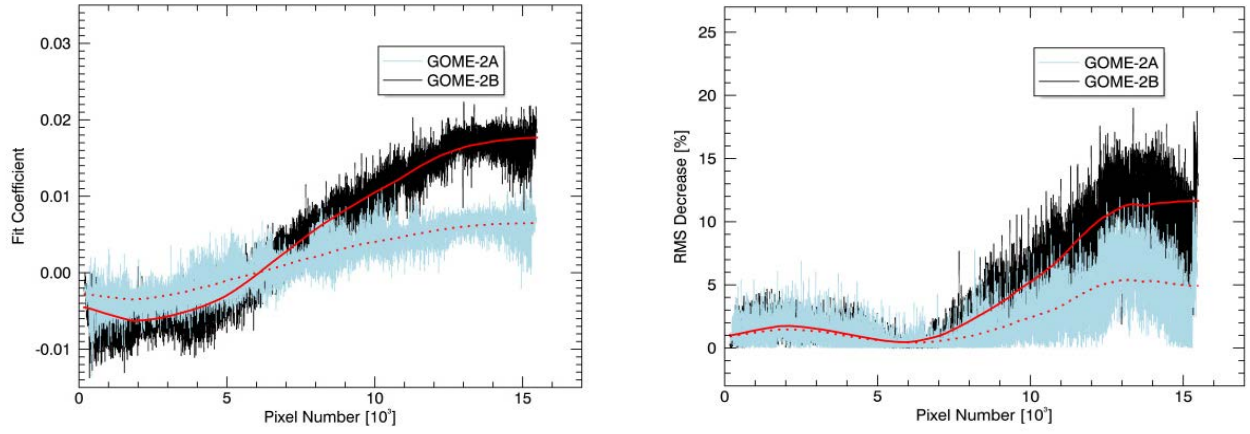

Figure 3. Changes of GOME-2 slit function width along orbit 32636 on 1 February 2013 (left) and the impact on the retrieval RMS error (right). Red lines provide the boxcar average for GOME-2A (dotted) and GOME-2B (solid). A fit coefficient of 1×10^{-2} corresponds to a change in the slit function width of $\sim 2.8 \times 10^{-3}$ nm in the left panel.

4.3.2 In-orbit variations

To correct for the in-orbit variations of GOME-2 slit function, a "resolution correction function" (Azam et al., 2015) is included as an additional cross-section in the DOAS fit (see Table 1). The cross-section is derived by dividing a high-resolution solar spectrum (Chance and Kurucz, 2010) convolved with a stretched preflight GOME-2 slit function (see Sect. 4.3.1) by itself but convolved with a slightly modified slit function. Figure 3 shows an example of the fit coefficients and the influence on our DOAS retrieval on 1 February 2013. As shown in the left panel, the slit function width increases along the orbit by $\sim 2 \times 10^{-3}$ nm ($\sim$0.4%) for GOME-2A (see Beirle et al. 2017, Fig. 8 therein) and $\sim 5.2 \times 10^{-3}$ nm ($\sim$1%) for GOME-2B (a fit coefficient of 1×10^{-2} corresponds to a change in the slit function width of $\sim 2.8 \times 10^{-3}$ nm). This in-orbit broadening of the slit function is caused by the increasing temperature of the instrument along the orbit. Taking into account the in-orbit broadening in the DOAS fit decreases the retrieval RMS by up to 5% for GOME-2A and up to 12% for GOME-2B in Fig. 3 (right).

4.4 GOME-2 level 1b data

As described in Sect. 2, the level 0 to 1b processing by the PPF at EUMETSAT calculates the geolocation and calibration parameters and produces the calibrated level 1b (ir)radiances. Due to the incomplete removal of Xe-line contamination in the GOME-2B calibration key-data (calibration key-data is taken during the on-ground campaign and required as an input to the level 0 to 1b processing), artefacts at wavelength larger than 460 nm have been reported by Azam et al. (2015) for GOME-2B irradiances. Mainly focusing on the cleaning of contamination in the GOME-2B calibration key-data, a new version 6.1 of the GOME-2 level 0 to 1b processor has been activated from 25 June 2015 onwards (EUMETSAT, 2015). To study the impact of the new level 1b data on our GDP 4.9 algorithm using the 425-497 nm fitting window, the retrieval is analysed using both

Atmos. Meas. Tech. Discuss., https://doi.org/10.5194/amt-2018-235
Manuscript under review for journal Atmos. Meas. Tech.
Discussion started: 6 August 2018

Atmospheric Measurement Techniques Discussions

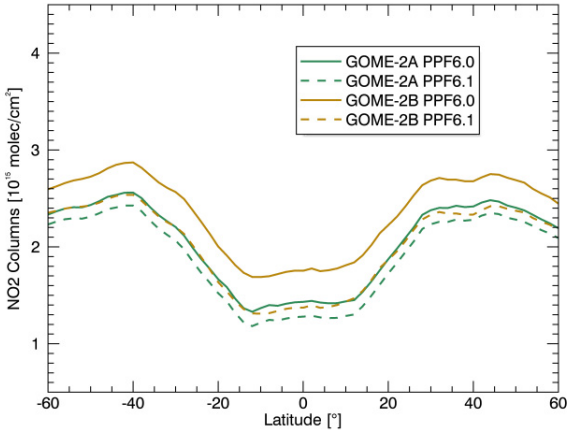

Figure 4. Monthly zonal average NO_2 columns (slant columns scaled by geometric AMFs) for GOME-2A (green) and GOME-2B (brown) using the new PPF 6.1 (dotted) and PPF 6.0 (solid) data in March 2015 over the Pacific (160°E-180°E).

the new version 6.1 (testing dataset provided by EUMETSAT for March 2015) and the previous version 6.0 data for the same period. Figure 4 presents a comparison of the retrieved NO_2 columns over the Pacific for GOME-2A and GOME-2B. The application of the version 6.1 level 1b data slightly reduces the NO_2 columns by $\sim$1-1.5 $\times 10^{14}$ molec/cm^2 ($\sim$6-11%) for GOME-2A. A larger effect is observed for GOME-2B with a decrease of NO_2 columns by $\sim$3-4 $\times 10^{14}$ molec/cm^2 ($\sim$15-23%) and a reduction of RMS error by $\sim$27-33% (not shown). The stronger decrease of GOME-2B NO_2 columns leads to a better consistency between the datasets from GOME-2A and GOME-2B with an overall bias reduced from $\sim 3 \times 10^{14}$ molec/cm^2 to $\sim 1 \times 10^{14}$ molec/cm^2.

4.5 Comparison to QA4ECV data

The quality of the GDP 4.9 retrieval is evaluated using the GOME-2 NO_2 dataset from QA4ECV, which is a project aiming at quality-assured satellite products using a retrieval algorithm harmonised for GOME, SCIAMACHY, OMI and GOME-2. The GOME-2A NO_2 columns from QA4ECV (version 1.1) for the years 2007-2015 have shown an improved quality over previous datasets (Zara et al., 2018). Table 1 gives an overview of the DOAS settings used in the QA4ECV project. Figure 5 shows a comparison of the NO_2 columns over the Pacific from the GDP 4.8 algorithm, the GDP 4.9 algorithm, and the QA4ECV data for February 2007. For comparison, only ground pixels with solar zenith angle smaller than 80° are considered. The GDP 4.8 dataset has been adjusted using a 220K Vandaele et al. (2002) NO_2 cross-section to remove the influence of temperature dependency of NO_2 cross-section (see discussion in Sect. 4.1). Compared to the GDP 4.8 dataset, the improved DOAS retrieval in the GDP 4.9 increases the NO_2 columns by $\sim$1-3 $\times 10^{14}$ molec/cm^2 (up to 27%). Compared to the QA4ECV product, a good overall consistency is found with the GDP 4.9 dataset at all latitudes considering the different DOAS settings such as fitting window, offset correction, and slit function characterisation.

Atmos. Meas. Tech. Discuss., https://doi.org/10.5194/amt-2018-235
Manuscript under review for journal Atmos. Meas. Tech.
Discussion started: 6 August 2018

Atmospheric Measurement Techniques Discussions

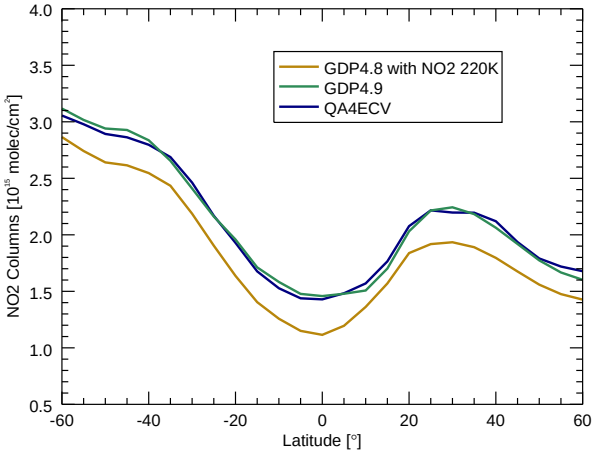

Figure 5. Comparisons of monthly zonal average NO_2 columns (slant columns scaled by geometric AMFs) from the operational GDP 4.8 product (but retrieved using a 220K NO_2 cross-section from Vandaele et al. 2002) (brown), the improved GDP 4.9 algorithm (green), and the QA4ECV dataset (blue) over the Pacific (160°E-180°E) in February 2007 for GOME-2A.

Figure 6 presents the time series of calculated slant column errors from the three datasets, following a statistical method to analyze the NO_2 slant column uncertainty for GOME-2 (Valks et al., 2011, Sect. 6.1 therein). The slant column errors, calculated as variations of NO_2 measurements within small boxes (2°×2°) over the tropical Pacific (20°S-20°N, 160°E-180°E), increase for all the three datasets as a result of instrument degradation (Dikty et al., 2011). Mainly driven by the use of a wider fitting window with stronger absorptions, smallest slant column errors are found by the GDP 4.9 algorithm, e.g., 23.8% smaller than from the GDP 4.8 and 13.5% smaller than from the QA4ECV dataset in February 2007, with an increasing difference with time for the QA4ECV dataset (27.9% in December 2015).

5 New stratosphere-troposphere separation

The calculation of tropospheric NO_2 requires an estimation and removal of the stratospheric contribution to the initial total NO_2 columns. In our GDP 4.9 retrieval, the stratosphere-troposphere separation algorithm STREAM (Beirle et al., 2016) has been adapted to GOME-2 measurements. Belonging to the modified reference sector method, STREAM uses initial total NO_2 columns with negligible tropospheric contribution, i.e., unpolluted measurements at remote areas and cloudy measurements at medium altitudes, to derive the stratospheric NO_2 columns. Based on a tropospheric NO_2 climatology and the GOME-2 cloud product, STREAM calculates weighting factors for each satellite pixel to define the contribution of initial total columns to the stratospheric estimation: potentially polluted pixels are weighted low instead of being totally masked out in the GDP 4.8 spatial filtering method; cloudy observations at medium altitudes are given higher weights because they directly provide the stratospheric information; the weights are further adjusted in a second iteration if pixels suffer from large biases in the tropospheric residues. Depending on these weighting factors, stratospheric NO_2 fields are derived by weighted convolution on the daily

Atmos. Meas. Tech. Discuss., https://doi.org/10.5194/amt-2018-235
Manuscript under review for journal Atmos. Meas. Tech.
Discussion started: 6 August 2018

Atmospheric Measurement Techniques Discussions

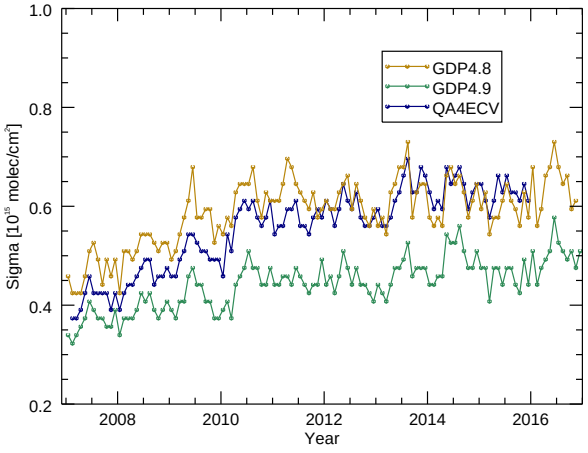

Figure 6. Temporal evolution of the NO_2 slant columns errors from the operational GDP 4.8 product (brown, January 2007-December 2016), the improved GDP 4.9 algorithm (green, January 2007-December 2016), and the QA4ECV dataset (blue, February 2007-December 2015) for GOME-2A, using deviations of NO_2 slant columns from box ($2°\times2°$) mean values over the tropical Pacific (20°S-20°N, 160°E-180°E).

initial total columns using convolution kernels. The convolution kernels are wider at lower latitudes due to the longitudinal homogeneity assumption of stratospheric NO_2 and narrower at higher latitudes to reflect the stronger natural variations. To remove the biases in the weighted convolution resulting from the large latitudinal gradients, a latitudinal correction is applied on the initial total columns: the latitudinal dependencies of initial total NO_2 are calculated over the clean Pacific, removed from the initial total NO_2 before weighted convolution, and added back to the estimated stratospheric columns afterwards. However, we found that longitudinal variations of NO_2 concentration resulted in biases in the latitudinal correction and hence in the stratospheric estimation. For the adaptation of STREAM to GOME-2 measurements, the performance of STREAM is analysed using synthetic GOME-2 NO_2 observations (see Sect. 5.1) and an improved latitudinal correction is applied (see Sect. 5.2).

5.1 Performance of STREAM

To test the performance of STREAM for GOME-2, simulated NO_2 fields from the C-IFS-CB05-BASCOE (referred to as C-IFS throughout this work) experiment (Huijnen et al., 2016) are applied. The C-IFS model is a combination of tropospheric chemistry module in the Integrated Forecast System (IFS, with current version based on the Carbon Bond chemistry scheme, CB05) of the European Centre for Medium-Range Weather Forecasts (ECMWF) and stratospheric chemistry from the Belgian Assimilation System for Chemical ObsErvations (BASCOE) system. Based on one year of C-IFS data (2009) at a resolution of 0.75°lon×0.75°lat, synthetic initial total columns V_{init} are calculated as:

$$V_{init} = \frac{S}{M_{strat}} = \frac{V_{total} \times M_{total}}{M_{strat}} \tag{7}$$

(see Eq. (2)). Modelled NO_2 slant columns S are based on the total vertical columns V_{total} from C-IFS with interpolation to match the GOME-2 centre pixel coordinate and measurement time. Total AMFs M_{total} and stratospheric AMFs M_{strat} are

Atmos. Meas. Tech. Discuss., https://doi.org/10.5194/amt-2018-235
Manuscript under review for journal Atmos. Meas. Tech.
Discussion started: 6 August 2018

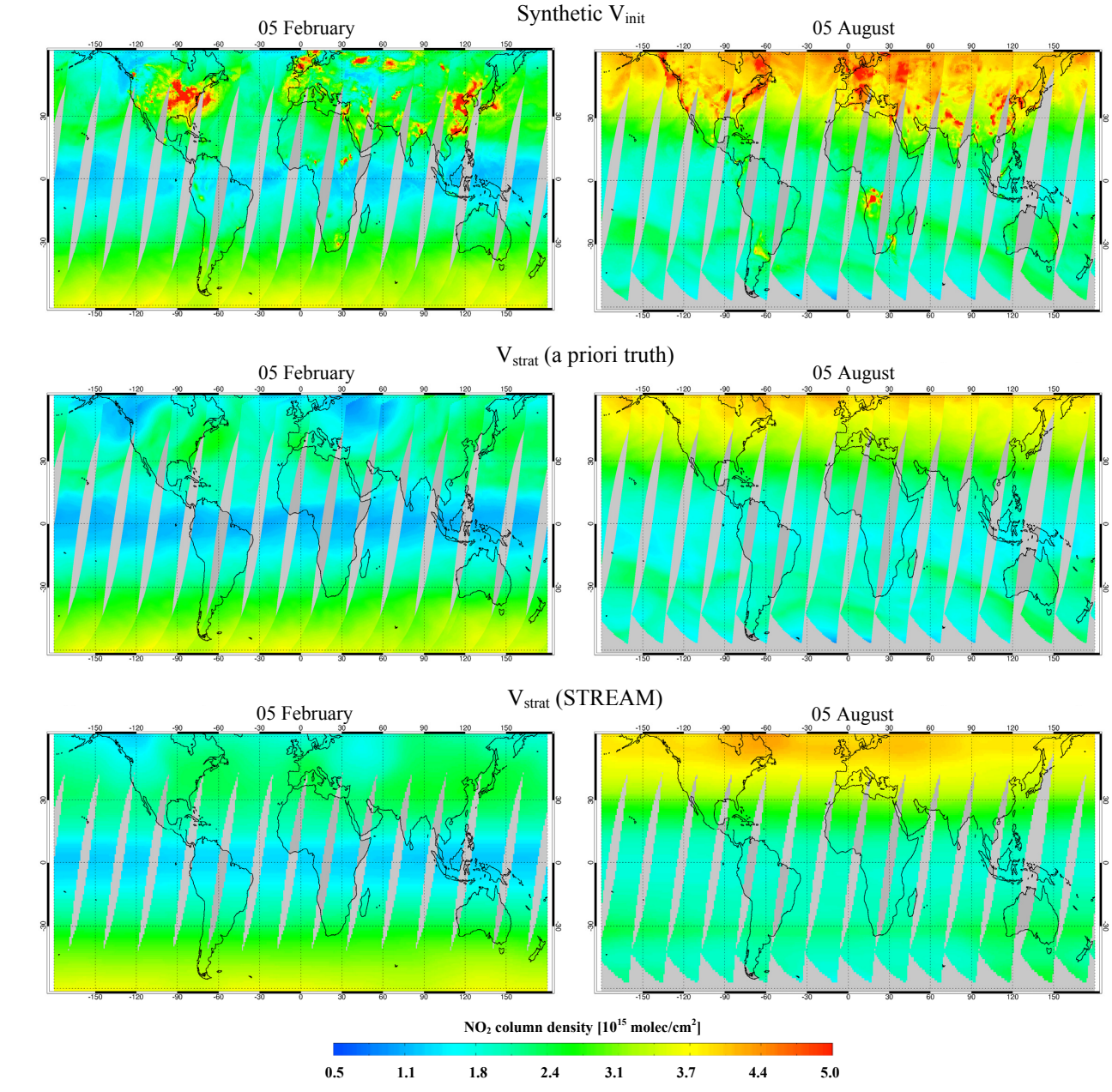

Figure 7. Synthetic initial total NO_2 columns (top), a priori stratospheric columns from C-IFS (center), and estimated stratospheric columns from STREAM (bottom) on 05 February (left) and 05 August (right) 2009.

derived using Eq. (3)-(5) with surface properties and cloud information from GOME-2 orbital data and with C-IFS a priori NO_2 profiles for the whole atmosphere and between the tropopause (defined by a latitude-dependent parameterization with

Atmos. Meas. Tech. Discuss., https://doi.org/10.5194/amt-2018-235
Manuscript under review for journal Atmos. Meas. Tech.
Discussion started: 6 August 2018

the tropopause height ranging from 270 hPa for arctic to 92 hPa for tropics) and the top of the atmosphere, respectively. The performance of STREAM is evaluated by applying the synthetic initial total NO_2 columns and comparing the estimated stratospheric NO_2 columns with the a priori truth (stratospheric fields from C-IFS integrated between the tropopause and the top of the atmosphere).

Figure 7 displays the synthetic initial total columns from C-IFS, the modelled stratospheric columns, and the estimated stratospheric columns from STREAM on 5 February and 5 August 2009. The result from STREAM presents an overall smooth stratospheric pattern with a strong latitudinal and seasonal dependency resulting from photochemical changes and dynamical variabilities. Because the stratospheric values over polluted regions are taken from the clean measurements at the same latitude, the stratospheric and tropospheric contribution over polluted regions is well separated by STREAM, especially in the northern hemisphere. Due to the latitude-dependent definition of convolution kernels, STREAM conserves the latitudinal gradients of stratospheric NO_2 at low latitudes and identifies certain strong stratospheric variations at high latitudes, e.g., in the polar vortex on 5 February. However, smaller structures in the synthetic initial total columns, for instance, resulting from the diurnal variation of NO_2 across an orbital swath, are aliased into the troposphere by STREAM due to the use of convolution kernels.

Figure 8 (top) shows the differences in estimated (Fig. 7 bottom) and a priori (Fig. 7 center) stratospheric NO_2. Overall, the stratospheric columns estimated from STREAM show a good agreement with the modelled truth with a slight overestimation, e.g., by $\sim$1-2 $\times 10^{14}$ molec/cm^2 over low latitudes for both days. Larger differences are found at higher latitudes, especially in winter, e.g., by $\sim 5 \times 10^{14}$ molec/cm^2 over eastern Europe and over the North Pacific (west of Canada) on 5 February. The strong longitudinal variations of NO_2 over these regions in the a priori truth (Fig. 7 center) can not be completely captured by STREAM (Fig. 7 bottom), which is a general limitation of the modified reference sector method. Note that these larger differences are reduced to $\sim 2 \times 10^{14}$ molec/cm^2 in monthly averages (not shown). The found deviations are in agreement with the uncertainty estimates in Beirle et al. (2016).

5.2 Improved latitudinal correction

In Fig. 8 (top), larger differences are noticeable over the subtropical regions in winter for both days, primarily related to the latitudinal correction used in STREAM. As described in the previous Sect. 5, the latitudinal correction is applied by determining the latitudinal dependencies of total NO_2 over the clean Pacific, removing the latitudinal dependencies before convolution and adding it back to the estimated stratospheric columns. However, longitudinal variations of total NO_2, for instance, enhanced total NO_2 columns over the Pacific (compared to the Atlantic Ocean) at 15°N-30°N on 5 February 2009 (Fig. 7 top left), introduce biases in the stratospheric NO_2 columns. Therefore, an improved latitudinal correction is introduced to reduce the biases over the subtropics. The new latitudinal correction determines the latitudinal dependencies of total NO_2 based on clean measurements in the whole latitude band (the median of lowest NO_2 columns for each 1° latitude band). Figure 8 (bottom) shows the difference for the estimated stratospheric NO_2 using the improved latitudinal correction. For both days, the application of the new latitudinal correction in STREAM largely removes the biases over the subtropics in Fig. 8 (top).

Applying the improved STREAM on GOME-2 data, Fig. 9 presents the initial total columns from GOME-2 and the stratospheric NO_2 calculated with STREAM and with the spatial filtering method used in the GDP 4.8 algorithm (see Sect. 3)

Atmos. Meas. Tech. Discuss., https://doi.org/10.5194/amt-2018-235
Manuscript under review for journal Atmos. Meas. Tech.
Discussion started: 6 August 2018

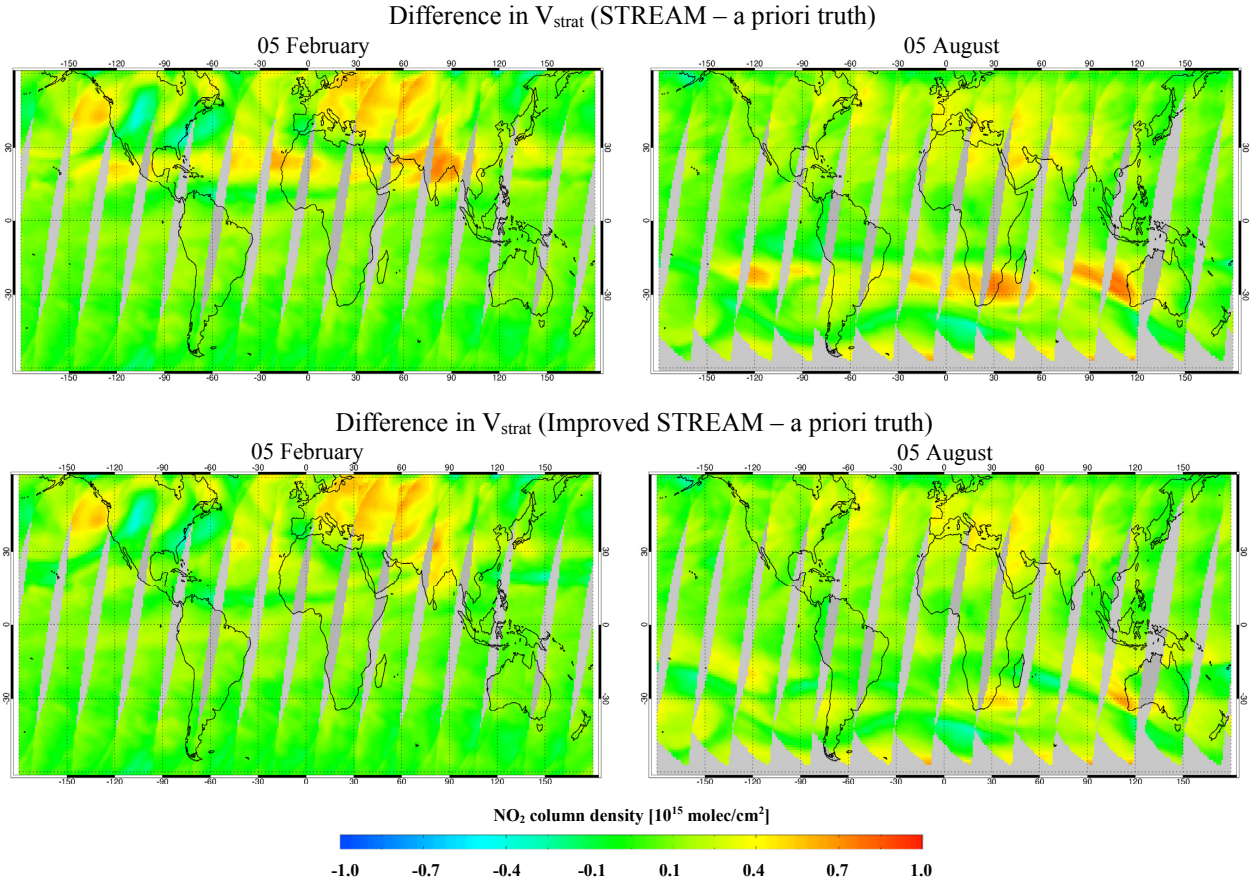

Figure 8. Difference in the stratospheric NO_2 columns estimated from STREAM and modelled by C-IFS on 5 February (top left) and 5 August (top right) 2009. Bottom panels show for STREAM with improved latitudinal correction.

in February and August 2009. For both months, the results calculated with STREAM and with the spatial filtering method show similar global structures. Since the spatial filtering method applies a fixed pollution mask to remove the potentially polluted regions (tropospheric NO_2 larger than 1×10^{15} molec/cm^2), moderately polluted pixels with tropospheric NO_2 up to 1×10^{15} molec/cm^2 still contribute to the stratospheric estimation. Therefore, enhanced stratospheric NO_2 by more than 5×10^{14} molec/cm^2 is found over polluted regions, e.g., Middle East, China, central Africa, southern Africa, and Australia in Fig. 9 (bottom). This overestimation is largely removed by STREAM in Fig. 9 (center).

Atmos. Meas. Tech. Discuss., https://doi.org/10.5194/amt-2018-235
Manuscript under review for journal Atmos. Meas. Tech.
Discussion started: 6 August 2018

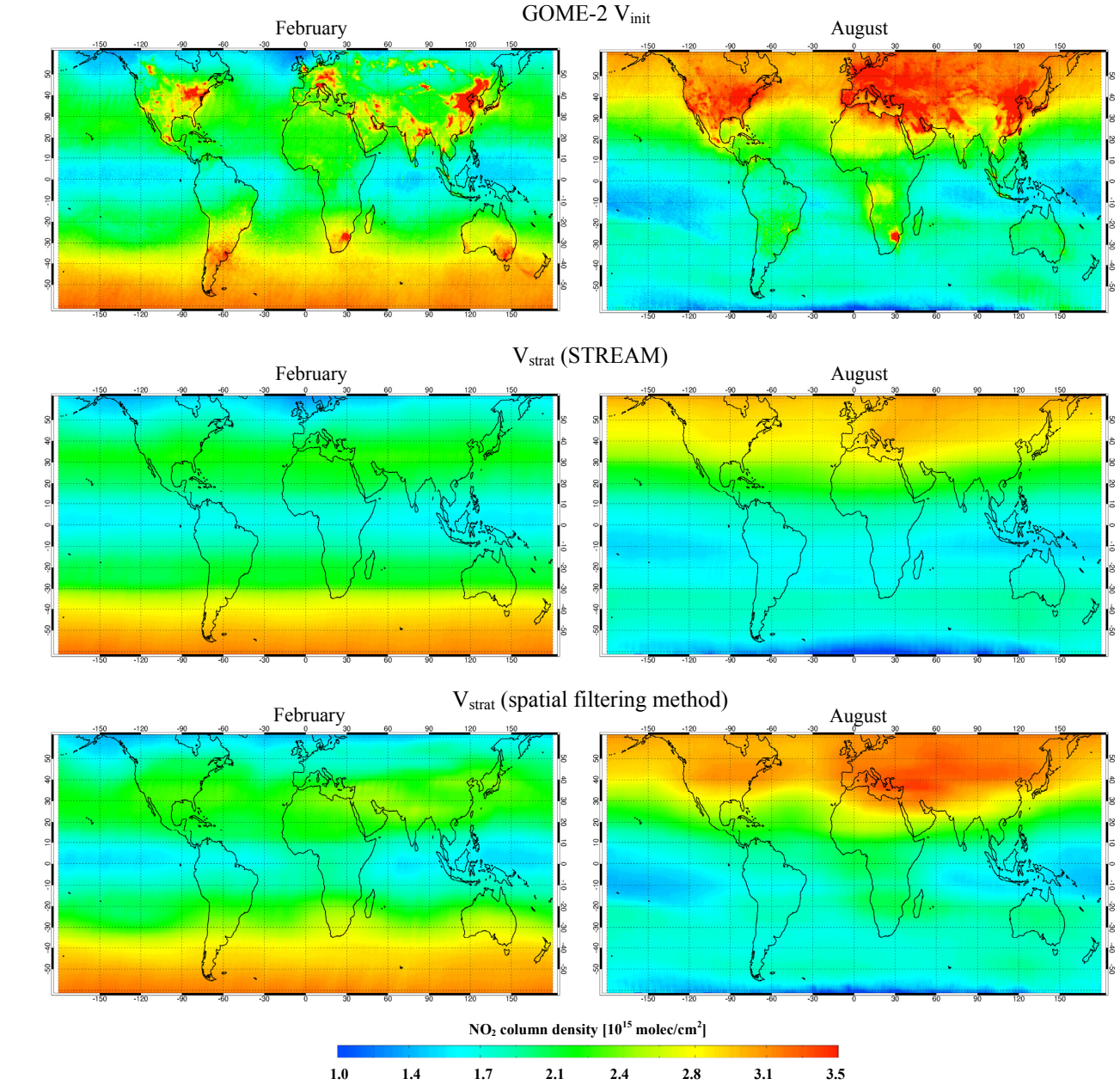

Figure 9. GOME-2 initial total NO_2 columns (top) and stratospheric NO_2 columns retrieved from the improved STREAM algorithm (center) and from the spatial filtering method used in GDP 4.8 (bottom), measured by GOME-2A in February (left) and August (right) 2009.

Atmos. Meas. Tech. Discuss., https://doi.org/10.5194/amt-2018-235
Manuscript under review for journal Atmos. Meas. Tech.
Discussion started: 6 August 2018

Atmospheric Measurement Techniques Discussions

Table 2. Main settings of AMF calculation method and input data discussed in this study.

	GDP 4.8	GDP 4.9 (this work)
RTM	LIDORT v2.2+	VLIDORT v2.7
Surface albedo	TOMS/GOME LER Boersma et al. (2004)	GOME-2 Min-LER v2.1 Tilstra et al. (2017b)
A priori profile	Monthly MOZART-2 (1.875°×1.875°)	Daily TM5-MP (1°×1°)

6 Improvements to NO_2 AMF calculation

6.1 RTM

As summarized in Table 2, updated box-AMFs are calculated using the linearised vector code VLIDORT (Spurr, 2006) version 2.7. VLIDORT applies the discrete ordinates method to generate simulated intensity and analytic intensity derivatives with respect to atmospheric and surface parameters (i.e. weighting functions). Box-AMFs m_l (see Eq. (3)) are determined as:

$$m_l = \frac{\partial \ln I}{\partial \tau_{NO_2,l}} = \frac{\frac{\partial I}{\partial \tau_{NO_2,l}} \cdot \tau_{NO_2,l}}{I \cdot \tau_{NO_2,l}} \tag{8}$$

with I the simulated top-of-atmosphere radiance, $\tau_{NO_2,l}$ the absorption optical thickness of NO_2 at layer l, and term $\frac{\partial I}{\partial \tau_{NO_2,l}} \cdot \tau_{NO_2,l}$ the NO_2 profile weighting function. Compared to the scalar (intensity-only) LIDORT code, VLIDORT provides more realistic modelling results with a treatment of light polarisation, which affects the tropospheric AMFs by up to 4%.

The box-AMFs for each layer are calculated for the mid-point wavelength of fitting window (461 nm) and stored in a LUT as a function of GOME-2 viewing geometry, surface pressure, and surface albedo. Compared to the LUT used in the GDP 4.8, a new LUT is calculated with an increased number of reference points, e.g., for surface pressure (from 10 to 16) and for surface albedo (from 10 to 14), as well as vertical layers (from 24 to 60) to reduce the interpolation error (Lorente et al., 2017), leading to differences in tropospheric AMFs by up to 2%.

6.2 Surface albedo

Surface albedo is an important parameter for an accurate retrieval of NO_2 columns and cloud properties. The sensitivity of backscattered radiance to the boundary layer NO_2 is strongly related to the surface albedo, especially over polluted areas. In the GDP 4.9, the surface LER climatology based on TOMS/GOME data (Boersma et al., 2004) has been replaced by one based on GOME-2 observations (Tilstra et al., 2017b). Using the degradation-corrected GOME-2 level 1 measurements, the GOME-2 surface LER is derived by matching the measurements in a pure Rayleigh scattering atmosphere without cloud. Compared to the TOMS/GOME LER climatology, the GOME-2 surface LER (version 2.1) dataset takes advantage of newer observations for 2007-2013, an increased spatial resolution of 1.0°lon×1.0°lat for standard grid cells and 0.25°lon×0.25°at coastlines (Tilstra et al., 2017a), and an improved treatment of cloud contaminated cells over the ocean.

Atmos. Meas. Tech. Discuss., https://doi.org/10.5194/amt-2018-235
Manuscript under review for journal Atmos. Meas. Tech.
Discussion started: 6 August 2018

Atmospheric Measurement Techniques Discussions

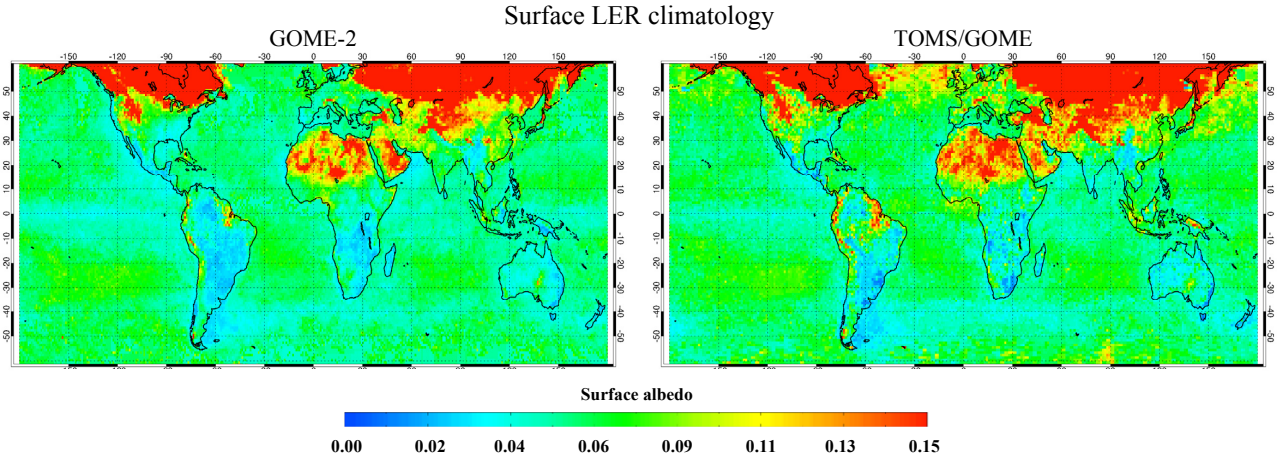

Figure 10. Map of surface LER data for 440 nm in February based on GOME-2 observations for 2007-2013 (Tilstra et al., 2017b) (left) and TOMS/GOME data for 1979-1993 (right).

Figure 10 shows the surface LER data from the GOME-2 and TOMS/GOME observations for 440 nm in February. A good overall consistency is found between the two LER datasets, in particular over the ocean. Larger differences are found over certain snow or ice areas, like Russia and southern Canada, which can be attributed to changes in snow or ice cover during the different measurement periods of the two LER datasets. Increased spatial resolution for the GOME-2 LER version 2.1 dataset enables a better representation of surface features for the land-sea boundaries, e.g., coasts around western Europe and eastern China. Improvements in the GOME-2 LER algorithm (Tilstra et al., 2017b) decreases the surface LER values over regions with persistent clouds, e.g., the North Atlantic Ocean and the North Pacific Ocean at middle latitudes. Systematic differences in the LER climatologies are also caused by the different overpass time, observing geometry, and radiometric calibration of the instruments.

Figure 11 illustrates the influence of the updated surface LER at 440 nm on the retrieved tropospheric NO_2 columns in February 2008. The difference over the ocean is very small. Larger effects are noticed primarily under polluted conditions with positive differences, e.g., over parts of central Europe, Russia or USA, and negative values, e.g., over parts of South Africa, India or China. The differences in the retrieved tropospheric NO_2 columns are consistent with the changes in the surface LER. For example, the GOME-2 surface LER over central Europe is $\sim$0.012 smaller than TOMS/GOME data, and a lower sensitivity to tropospheric NO_2 is therefore assumed in the AMF calculation. This results in a decrease in the AMF and hence an increase in the retrieved tropospheric NO_2 column by $\sim 7 \times 10^{14}$ molec/cm^2 ($\sim$12%). Vice versa, an increase of the surface LER values by $\sim$0.018 over the Yangtze River region in eastern China leads to a reduction of tropospheric NO_2 columns by $\sim 4 \times 10^{15}$ molec/cm^2 ($\sim$15%).

It should be noted that the AMFs are calculated for 461 nm in the GDP 4.9 (425-497 nm wavelength window) instead of 440 nm in the GDP 4.8 (with 425-450 nm wavelength window), therefore the corresponding surface LER values are 463 nm

Atmos. Meas. Tech. Discuss., https://doi.org/10.5194/amt-2018-235
Manuscript under review for journal Atmos. Meas. Tech.
Discussion started: 6 August 2018

Atmospheric Measurement Techniques Discussions

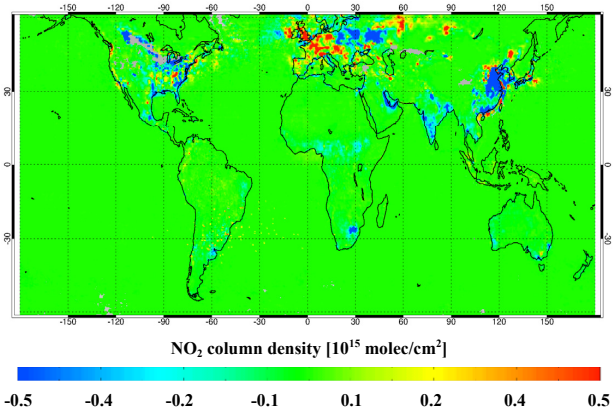

Figure 11. Difference in tropospheric NO_2 columns for clear-sky conditions (cloud radiance fraction smaller than 0.5) for February 2008 retrieved using the GOME-2 surface LER climatology version 2.1 and the LER climatology based on TOMS/GOME data at 440 nm.

are used. The surface LER values at 463 nm are higher by up to 0.02 over desert areas and lower by up to 0.02 over the ocean and the snow or ice areas, which result in differences of up to 5% in the calculated AMFs.

The surface LER climatology from Kleipool et al. (2008) derived from OMI measurements for 2004-2007 has been widely used in satellite NO_2 retrievals (e.g., Boersma et al., 2011; Barkley et al., 2013; Bucsela et al., 2013). An important advantage of using the GOME-2 LER climatology with respect to the OMI LER dataset in our retrieval is the consistency with the GOME-2 NO_2 observations, considering the illumination conditions, observation geometry, and instrumental characteristics.

6.3 A priori vertical profiles

The retrieved tropospheric NO_2 columns are sensitive to changes in the relative vertical distribution of the a priori NO_2 concentrations (i.e. profile shape). To improve the tropospheric AMF calculation, daily a priori NO_2 profiles are obtained with a resolution of 1°lon×1°lat from the chemical transport model TM5-MP (Huijnen et al., 2010; Williams et al., 2017). The TM5-MP profiles have been used in several studies to derive AMFs and tropospheric NO_2 columns (e.g., van Geffen et al., 2016; Lorente et al., 2017; Boersma et al., 2018).

Figure 12 shows the TM5-MP and MOZART-2 a priori NO_2 profiles for two pollution hot spots located in Brussels (Belgium, 50.9°N, 4.4°E) and Guangzhou (China, 23.1°N, 113.3°E) on one day in February and August 2009 as examples. Monthly profiles are shown for MOZART-2, and profiles for the given days are shown for TM5-MP. Large differences between the a priori NO_2 profile shapes from TM5-MP and MOZART-2 are found for both cities. These differences are the result of the different chemical mechanism, transport scheme, and emission inventory employed by the model, the different spatial resolution, and the use of daily vs. monthly profiles. In TM5-MP, the use of updated NO_x emissions from the MACCity inventory (Granier et al., 2011) produces more realistic profiles. Improvement in the spatial resolution gives a more accurate

Atmos. Meas. Tech. Discuss., https://doi.org/10.5194/amt-2018-235
Manuscript under review for journal Atmos. Meas. Tech.
Discussion started: 6 August 2018

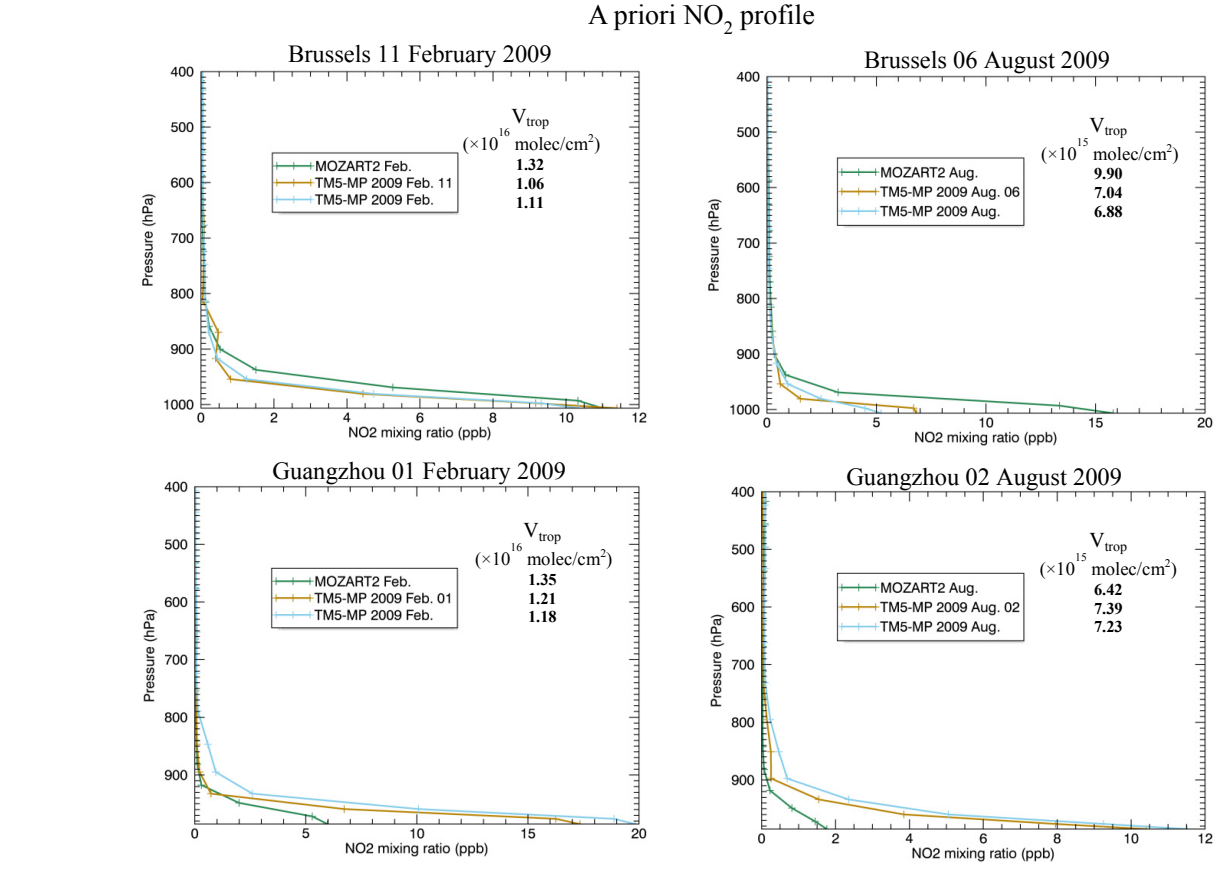

Figure 12. Examples of a priori NO_2 profiles for Brussels (top) and Guangzhou (bottom) on a given day in February (left) and August (right) 2009. Monthly profiles are shown for MOZART-2 (green), and daily profiles on the given days are shown for TM5-MP (brown) together with the monthly average profiles calculated for TM5-MP (blue). The tropospheric NO_2 columns retrieved using each a priori NO_2 profile are also given.

description of the NO_2 gradient and transport. The use of daily profiles provides a better description of the temporal NO_2 variation, especially for regions dominated by emission and transport like Brussels and Guangzhou.

In Fig. 12, the tropospheric NO_2 columns retrieved for the individual days using TM5-MP and MOZART-2 a priori NO_2 profiles are also reported. Taking Brussels on 11 February 2009 (Fig. 12 top left) as an example, the smaller boundary layer concentration modelled by TM5-MP (less steep profile shape) leads to an increase in the tropospheric AMF and hence a decrease in the retrieved tropospheric NO_2 columns by 2.6×10^{15} molec/cm^2 (19.7%). Figure 13 presents a comparison of the monthly averaged tropospheric NO_2 columns retrieved using daily TM5-MP and monthly MOZART-2 a priori NO_2 profiles in February and August 2009. The application of the daily TM5-MP a priori NO_2 profiles affects the tropospheric NO_2 columns by more than 1×10^{15} molec/cm^2 mostly over polluted regions with enhanced NO_2 in the boundary layer, e.g., with an increase of tropospheric NO_2 over parts of China, India, and South Africa, and a decrease over parts of eastern US, Europe, and Japan.

Atmos. Meas. Tech. Discuss., https://doi.org/10.5194/amt-2018-235
Manuscript under review for journal Atmos. Meas. Tech.
Discussion started: 6 August 2018

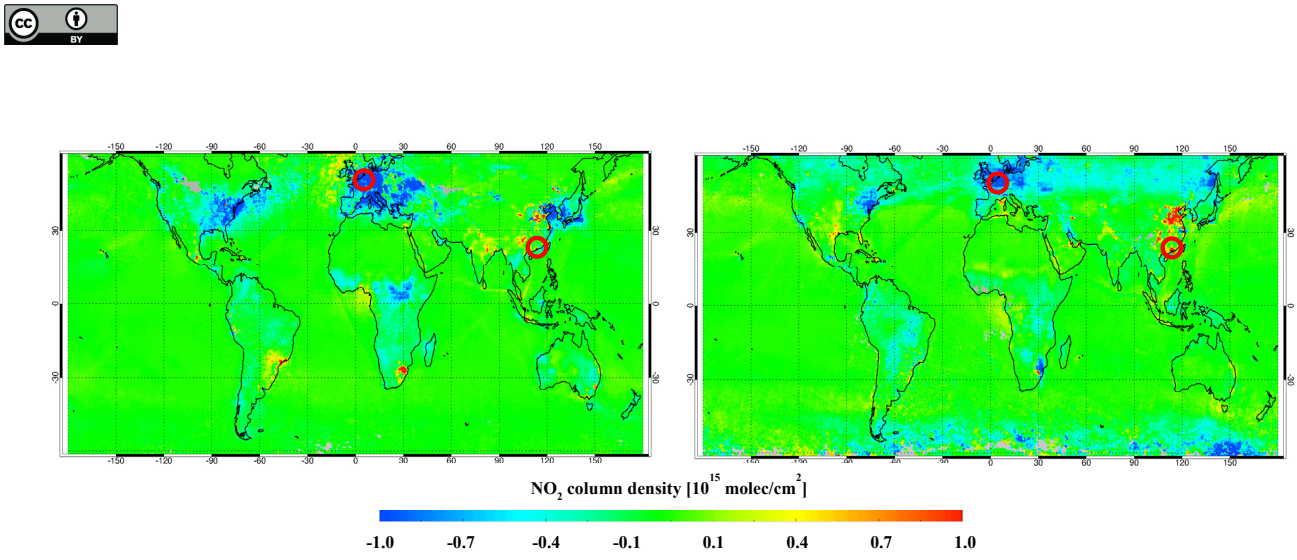

Figure 13. Difference in tropospheric NO_2 columns for clear-sky conditions (cloud radiance fraction smaller than 0.5) retrieved using daily TM5-MP and monthly MOZART-2 a priori NO_2 profiles for February (left) and August (right) 2009. Red circles indicate locations in Fig. 12.

To analyse the effect of using daily vs. monthly profiles, the tropospheric NO_2 columns are also retrieved using the monthly average TM5-MP profiles, as shown in Fig. 12. Differences in the profile shape of daily and monthly profiles are mainly related to the variations in the meteorology (Nüß et al., 2006). For both cities, the use of monthly TM5-MP profiles affects the tropospheric NO_2 columns by more than 1.5×10^{14} molec/cm^2. For the example of Brussels on 11 February 2009 (Fig. 12 top left), the use of monthly profiles increases the tropospheric NO_2 columns by 5×10^{14} molec/cm^2 (4.7%). A comprehensive analyse of the effect of using a priori NO_2 profiles from different chemistry transport models on the retrieved tropospheric NO_2 will be described in a subsequent paper.

6.4 Cloud parameters

For cloudy scenarios, the retrieval of tropospheric NO_2 component is affected by the cloud parameters due to the variation of albedo, reflecting boundary, and photon path. As discussed in Sect. 3, the cloudy-sky AMFs are calculated with the independent pixel approximation using GOME-2 derived cloud parameters: cloud fraction, cloud pressure, and cloud albedo. The OCRA/ROCINN algorithms (Loyola et al., 2007, 2011) are applied to calculate the GOME-2 cloud parameters: OCRA derives the cloud fraction by separating a spectral scene into cloudy contribution and cloud-free background and ROCINN calculates the cloud pressure and the cloud albedo by comparing simulated and measured radiance in and near the O_2 A-band.

In the GDP 4.9, a new version 3.0 of the OCRA/ROCINN algorithms (Lutz et al., 2016; Loyola et al., 2018) is used. The new OCRA algorithm applies a degradation correction on the GOME-2 level 1 measurements as well as corrections for viewing angle and latitudinal dependencies. A new cloud-free background is constructed from six years of GOME-2A measurements from the years 2008-2013. The updated OCRA also includes an improved detection and removal of sun glint that affects most of the GOME-2 orbits. The new ROCINN algorithm applies a forward RTM calculation using updated surface

albedo climatology and spectroscopic data as well as a new inversion scheme based on Tikhonov regularization (Tikhonov and Arsenin, 1977; Doicu et al., 2010). The computation time of ROCINN is optimised with a smart sampling method (Loyola et al., 2016). Overall, the use of OCRA/ROCINN v3.0 shows an increase of cloud fraction and cloud pressure for nearly cloud-free situation with an improved cloud correction effect on the AMF calculation (Pinardi et al., 2015).

7 End-to-end GOME-2 NO_2 validation

The validation of NO_2 data derived from GOME-2 GDP algorithm is part of the validation activities done at BIRA-IASB in the AC-SAF context (Hassinen et al., 2016). An end-to-end validation approach is usually performed for each main release and summarized in validation reports that can be found on AC-SAF validation website (http://cdop.aeronomie.be/validation/valid-reports). This includes several steps, such as: (1) the DOAS analysis results, cloud properties retrievals, and AMF evaluations by confrontation of GOME-2 retrievals to other established satellite retrievals and AMF evaluations; (2) the stratospheric reference evaluation by comparison with correlative observations from ground-based zenith-looking DOAS spectrometers and from other nadir-looking satellites; and (3) the tropospheric and total NO_2 column data evaluation by comparison with correlative observations from ground-based multiple-axis DOAS (MAXDOAS) and Direct Sun spectrometers (Pinardi et al., 2014). In this paper, we focus on the last point: the validation of tropospheric data with BIRA-IASB ground-based MAXDOAS data.

The MAXDOAS instruments collect scattered sky light in a series of line-of-sight angular directions extending from the horizon to the zenith. High sensitivity towards absorbers near the surface is obtained for the smallest elevation angles, while measurements at higher elevations provide information on the rest of the column. This technique allows the determination of vertically resolved abundances of atmospheric trace species in lowermost troposphere (Hönninger et al., 2004; Wagner et al., 2004; Wittrock et al., 2004; Heckel et al., 2005). Here the bePRO retrieval code (Clémer et al., 2010; Hendrick et al., 2014; Vlemmix et al., 2015) is used to retrieve tropospheric columns and low tropospheric profiles (up to 3.5 km with about 2 to 3 degrees of freedom).

As summarised in Table 3, a set of MAXDOAS stations (Beijing, Bujumbura, Observatoire de Haute Provence (OHP), Reunion, Uccle, and Xianghe) is providing interesting test cases for GOME-2 sensitivity to tropospheric NO_2. Indeed Beijing and Uccle are typical urban stations, Xianghe is a suburban station ($\sim$60 km from Beijing), Bujumbura and Reunion are small cities in remote regions, and OHP is largely rural but occasionally influenced by polluted air masses transported from neighboring cities. These different station types are important in the validation context as it is generally expected that urban stations are underestimated by the satellite data, due to the averaging of a local source over a pixel size (80×40 km^2 for GOME-2) larger than the horizontal sensitivity of the ground-based measurements which is about few to tens of km (Irie et al., 2011; Wagner et al., 2011; Ortega et al., 2015). In this context, MAXDOAS data is already better than in-situ measurements with an extended horizontal and vertical sensitivity, more similar to the satellite sensitivity, but differences in sampling and sensitivity still remain and explain part of the biases highlighted by validation exercises. Several validation studies show significant underestimation of tropospheric trace gases, such as NO_2, from satellite observations over regions with strong spatial gradients in tropospheric pollution (e.g., Celarier et al., 2008; Kramer et al., 2008; Chen et al., 2009; Irie et al., 2012; Ma et al., 2013;

Atmos. Meas. Tech. Discuss., https://doi.org/10.5194/amt-2018-235
Manuscript under review for journal Atmos. Meas. Tech.
Discussion started: 6 August 2018

Atmospheric Measurement Techniques Discussions

Table 3. An overview of BIRA-IASB MAXDOAS datasets used in this study.

MAXDOAS station	period	position	description
Beijing	6/2008-4/2009	39.98°N, 116.38°E	urban polluted site in China
Bujumbura	12/2013-11/2016	3.38°S, 29.38°E	urban site in Burundi
OHP	3/2007-11/2016	43.94°N, 5.71°E	background site in southern France
Reunion	4/2016-11/2016	21°S, 55.3°E	urban site in Reunion Island
Uccle	4/2011-11/2016	51°N,4.36°E	urban polluted site in Belgium with a miniDOAS
Xianghe	3/2010-11/2016	39.75°N, 116.96°E	suburban polluted site in China

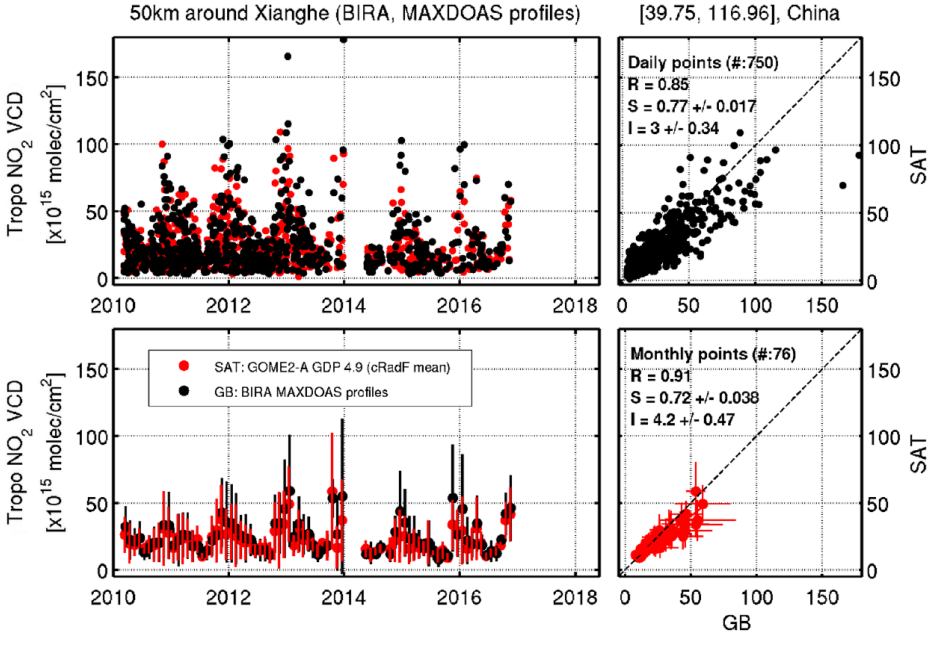

Figure 14. Daily (upper row) and monthly mean (lower row) time series and scatter plot of GOME-2A and MAXDOAS tropospheric NO_2 columns (mean value of all the pixels within 50km around Xianghe).

Wu et al., 2013; Kanaya et al., 2014; Wang et al., 2017; Drosoglou et al., 2017, 2018). Other possible explanations include the uncertainties in the applied satellite retrieval assumptions, such as the choices of surface albedo, a priori NO_2 profiles, or cloud and aerosol treatment (Boersma et al., 2004, 2011; Leitão et al., 2010; Heckel et al., 2011; Lin et al., 2014, 2015). The best agreement is generally obtained in the case of suburban and remote stations, but difficulties may arise when small local sources are present in a remote location, such as Reunion Island or Bujumbura (Pinardi et al., 2015; Gielen et al., 2017).

Atmos. Meas. Tech. Discuss., https://doi.org/10.5194/amt-2018-235
Manuscript under review for journal Atmos. Meas. Tech.
Discussion started: 6 August 2018

Atmospheric Measurement Techniques Discussions

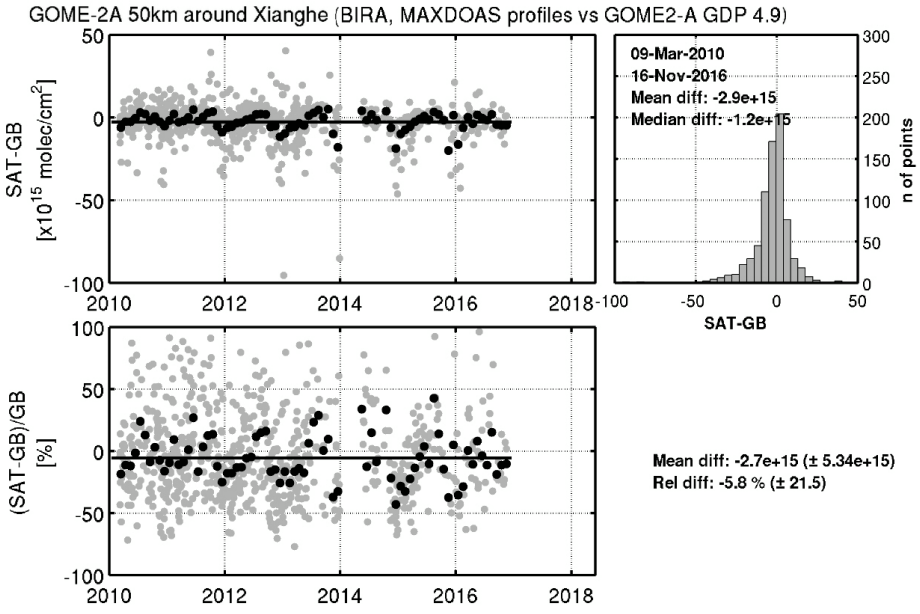

Figure 15. Daily (grey dots) and monthly mean (back dots) absolute and relative GOME-2A and MAXDOAS time series differences for the Xianghe station. The histogram of the daily differences is also given, with the mean and median difference, and the total time-series absolute and relative monthly differences are given outside the panels.

The same methodology as in the GDP 4.8 validation report (Pinardi et al., 2015) is used for the validation of this improved GDP 4.9 tropospheric NO_2 dataset: the satellite data are filtered for clouds (cloud radiance fraction smaller than 0.5) and the mean value of all the valid pixels within 50 km of the stations is compared to the ground-based value, interpolated to the satellite overpass time (9:30 local time). Figure 14 shows an example of the time-series and scatter plot of the daily and monthly means comparison between GDP 4.9 tropospheric NO_2 columns and ground-based MAXDOAS measurements in Xianghe, including the statistical information on the number of points, correlation coefficient, slope and intercept of orthogonal regression analysis. Figure 15 presents the daily and monthly mean absolute and relative differences of GDP 4.9 and ground-based measurements. As can be seen in Fig. 14 and 15, the seasonal variation in the tropospheric NO_2 columns is similarly captured by both observation systems with differences on average within $\pm 3 \times 10^{15}$ molec/cm^2 (median difference of -1.2×10^{15} molec/cm^2). Larger differences are observed on some days and months, in particular in winter when NO_2 and aerosol loadings are large. A relatively compact scatter is found, with a correlation coefficient of 0.91 and a slope of 0.72±0.04 for the orthogonal regression fit. These results are qualitatively similar to those obtained in previous validation exercises (Celarier et al., 2008; Kramer et al., 2008; Chen et al., 2009; Irie et al., 2012; Ma et al., 2013; Wu et al., 2013; Kanaya et al., 2014; Wang et al., 2017; Drosoglou et al., 2017, 2018). Similar figures for GDP 4.8 can be found on the AC-SAF validation website (http://cdop.aeronomie.be/validation/valid-results). Figure 16 reports the monthly mean absolute and relative differences for both

Atmos. Meas. Tech. Discuss., https://doi.org/10.5194/amt-2018-235
Manuscript under review for journal Atmos. Meas. Tech.
Discussion started: 6 August 2018

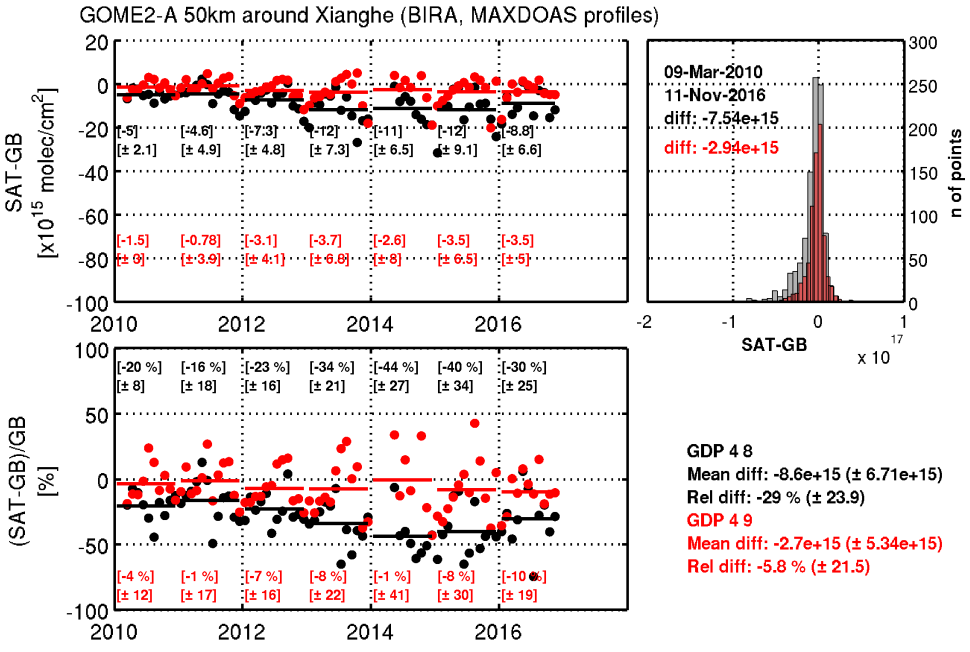

Figure 16. Absolute and relative differences of GOME-2A and MAXDOAS tropospheric NO_2 columns. The time-series presents the monthly mean differences for GDP 4.8 (black) and GDP 4.9 (red). The total mean differences values and standard deviations are given, as well as the yearly values. The histogram presents the daily differences over the whole time-series for the two products (grey for GDP 4.8 and red for GDP 4.9).

GDP 4.8 and GDP 4.9 for Xianghe station. The daily differences are also reported through the histogram panel. Similar figures as Fig. 14 and 16 for all the stations are gathered in Fig. S1-S4 in the supplement. From the figures, a better seasonal agreement between GDP 4.9 and MAXDOAS data is found for urban and suburban cases like Beijing, Uccle, and Xianghe. The absolute and relative differences for all the stations show a clear improvement compared to GDP 4.8 for both daily and monthly mean biases.

Table 4 summarizes the comparisons of mean biases and results of regression analysis at the 6 BIRA-IASB stations for GOME-2A and Table 5 for GOME-2B. As discussed in Pinardi et al. (2015), for background stations, the mean bias is considered as the best indicator of the validation results, due to the relatively small variability in the measured NO_2. In urban and suburban situations, the NO_2 variability is large enough and in this case, the correlation coefficient is a good indication of the linearity or coherence of the satellite and ground-based dataset, but larger difference in term of slope (closer to 0.5 than to 1 for urban cases) and of mean bias is also expected because satellite measurements smooth out the NO_2 hot spots. From Table 4, the relative differences in urban conditions such as in Beijing or Uccle decrease from -52-60% for GDP 4.8 to -43-47% for

Atmos. Meas. Tech. Discuss., https://doi.org/10.5194/amt-2018-235
Manuscript under review for journal Atmos. Meas. Tech.
Discussion started: 6 August 2018

Atmospheric Measurement Techniques Discussions

Table 4. Averaged Absolute Differences (AD, SAT-GB in 10^{15} molec/cm^2), Relative Differences (RD, (SAT-GB)/GB in %), standard deviation (STDEV), correlation coefficient R and regression parameters (slope S and intercept I) of the orthogonal regression for the monthly means GOME-2A tropospheric NO_2 product when comparing to MAXDOAS data. Values for GDP 4.9 (this study) are given and the values for GDP 4.8 are reported in brackets for comparison. Results for both the original comparisons and the smoothed comparisons (smo.) are reported.

	AD ± STDEV ($\times 10^{15}$); RD (%)	R	regression parameters
Beijing	-16±7.3; -47% [-21±4.5; -60%]	0.94 [0.95]	S=0.4±0.04, I=3.4±0.6 [S=0.58±0.06, I=-6.2±0.7]
Beijing (smo.)	-11±6.5; -37% [-16±6.3; -52%]	0.94 [0.96]	S=0.43±0.05, I= 4.4±0.6 [S=0.48±0.04, I= 0.11±0.5]
Bujumbura	-3.6±1.8; -76% [-3.7±1.1; -89%]	na [0.29]	na [S=0.1±0.05, I=0.012±0.12]
Bujumbura (smo.)	-1.9±1.2; -62% [-2.4±0.8; -84%]	na [0.51]	na [S=0.22±0.06, I=-0.18±0.1]
OHP	-0.9±1; -25% [-1.2±0.7; -45%]	0.4 [0.69]	S=0.25±0.06, I=1.2±0.1 [S=0.73±0.07, I=-0.5±0.1]
Reunion	-1.5±0.5; -64% [-1.9±0.4; -90%]	0.14 [0.23]	S=0.05±0.12, I=0.64±0.2 [S=0.06±0.06, I=0.12±0.08]
Reunion (smo.)	-0.4±0.4; -31% [-0.7±0.2; -77%]	0.15 [0.28]	S=0.12±0.25, I=0.06±0.09 [S=0.32±0.25, I=-0.01±0.2]
Uccle	-5±2.7; -43% [-6.2±3.7; -52%]	0.82 [0.49]	S=0.47±0.05, I=0.83±0.2 [S=0.35±0.08, I=1.1±0.4]
Uccle (smo.)	-3.8±2.8; -34% [-7.6±4.3; -57%]	0.75 [0.51]	S=0.45±0.05, I=0.15±0.05 [S=0.28±0.06, I=1.5±0.3]
Xianghe	-2.7±5.3; -5.8% [-9.2±7.1; -30%]	0.91 [0.86]	S=0.72±0.04, I=4.2±0.5 [S=0.63±0.04, I= 1.3±0.5]
Xianghe (smo.)	-6.1±8.8; -13% [-11±9.6; -32%]	0.92 [0.9]	S=0.52±0.03, I= 7.4±0.43 [S=0.48±0.03, I=4.3±0.5]

Table 5. Same as Table 4 but for GOME-2B product.

	AD ± STDEV ($\times 10^{15}$); RD (%)	R	regression parameters
Bujumbura	-2.8±0.9; -74% [-3.4±1; -87%]	0.14 [0.09]	S=0.05±0.06, I=0.7±0.12 [S=0.03±0.06, I=0.34±0.1]
Bujumbura (smo.)	-1.3±0.7; -57% [-2±0.8; -81%]	0.28 [0.35]	S=0.14± 0.06, I=0.06±0.04 [S=0.15±0.06, I=0.08±0.1]
OHP	-0.5±0.7; -17% [-1±0.6; -42%]	0.13 [0.52]	S=0.11±0.13, I=1.5±0.2 [S=0.82±0.2, I=-0.6±0.3]
Reunion	-0.8±0.3; -47% [-1.6±0.3; -86%]	0.56 [0.26]	S=0.71±0.4, I=-0.4±0.52 [S=0.08±0.06, I=0.13±0.09]
Reunion (smo.)	0.05±0.2; 6.7% [-0.5±0.2; -64%]	0.78 [0.14]	S=-2.5±0.8, I=-0.12±0.22 [S=0.38±0.6, I=0.004±0.5]
Uccle	-4.2±2.4; -40% [-5.6±3.1; -54%]	0.71 [0.71]	S=0.53±0.09, I=0.47±0.4 [S=0.64±0.1, I=-1.7±0.5]
Uccle (smo.)	-2.8±2.5; -29% [-6.8±3.4; -56%]	0.69 [0.73]	S=0.53±0.09, I=0.13±0.09 [S=0.52±,0.1 I= -1±0.4]
Xianghe	-3±9.4; -2.2% [-8.4±8.7; -26%]	0.87 [0.84]	S=0.49±0.05, I=9.6±0.66 [S=0.6±0.05, I=2.5±0.7]
Xianghe (smo.)	-6.4±13; -11% [-11±12; -27%]	0.89 [0.89]	S=0.38±0.03, I=11±0.6 [S=0.46±0.03, I=5.2±0.58]

GDP 4.9. In suburban conditions such as in Xianghe, the differences go from -30% to -6%. In remote (but in the city) cases such as in Reunion or Bujumbura, the differences go from -89-90% to -64-76%, while in background case such as in OHP, the differences decrease from -45% to -25%. A decrease of differences with similar magnitude is also found in Table 5.

For most stations, in addition of the tropospheric columns, MAXDOAS retrieved NO_2 profiles can also be exploited with satellite column averaging kernels (AK) to further investigate the impact of the satellite a priori NO_2 profiles in the comparison

Atmos. Meas. Tech. Discuss., https://doi.org/10.5194/amt-2018-235
Manuscript under review for journal Atmos. Meas. Tech.
Discussion started: 6 August 2018

differences (Eskes and Boersma, 2003). The satellite AK describes the vertical sensitivity of measurements to NO_2 concentrations and relates the MAXDOAS profiles to satellite column measurements by calculating the "smoothed MAXDOAS columns" as:

$$V_{MAXDOAS,smoothed} = \sum_{l} AK_{sat,l} \times x_{MAXDOAS,l}. \quad (9)$$

The smoothed MAXDOAS NO_2 columns $V_{MAXDOAS,smoothed}$ are derived for each day by convolving the layer (l)-dependent daily profile (interpolated to the satellite overpass time) $x_{MAXDOAS}$ expressed in partial columns with the satellite column averaging kernel AK_{sat}. In general, the use of satellite column AK takes into account the differences in vertical sensitivity between MAXDOAS and satellite measurements and hence improves the comparisons results, but this might not be the case at all the stations due to the different influence of the difference in the shape between the MAXDOAS retrieved profiles and the a priori NO_2 profiles used in the satellite retrievals.

The comparisons of satellite and smoothed MAXDOAS columns for the different stations are reported in the supplement (Fig. S5 and S6) and Table 4 and 5. The different impact of MAXDOAS smoothing on the two GDP products results from the different AK as parameters like surface albedo or a priori NO_2 profiles used in both satellite retrievals are quite different (see Sect. 6). In general, the use of smoothing reduces the MAXDOAS columns and thus reduces both the daily and monthly differences of satellite and MAXDOAS columns. From Table 4, when the satellite averaging kernels are used to remove the contribution of a priori NO_2 profile shape, the differences for GDP 4.9 are -34-37% in urban conditions, -13% in suburban, and -31% for Reunion Island. The results obtained here are coherent with other validation exercises at different stations and with other satellite products, where the NO_2 levels are underestimated by the satellite sensors, e.g., with differences of 5% to 25% over China (Ma et al., 2013; Wu et al., 2013; Wang et al., 2017; Drosoglou et al., 2018), mostly explained by the relatively low sensitivity of space-borne measurements near the surface, the a priori NO_2 profiles assumed for the AMF calculations, the gradient-smoothing effect, and the aerosol shielding effect. However, the differences in Bujumbura are still of -62%, because of the peculiar condition with the MAXDOAS being in a valley, close to the Tanganika lake, which always leads to a higher surface pressure for the satellite pixels due to the information coming from the a priori model. This is leading to large representation errors and uncertainties in the comparisons (Boersma et al., 2016) that needs to be investigated in more details.

8 Conclusions

NO_2 columns retrieved from measurements of the GOME-2 aboard the MetOp-A and MetOp-B platforms have been successfully applied in many studies. The abundance of NO_2 is retrieved from the narrow band absorption structures of NO_2 in the backscattered and reflected radiation in the visible spectral region. The current operational retrieval algorithm (GDP 4.8) for total and tropospheric NO_2 from GOME-2 was first introduced by Valks et al. (2011), and an improved algorithm (GDP 4.9) is described in this paper.

To calculate the NO_2 slant columns, a larger 425-497 nm wavelength fitting window is used in the DOAS fit to increase the signal-to-noise ratio. Absorption cross-sections are updated and a linear intensity offset correction is applied. The long-term

Atmos. Meas. Tech. Discuss., https://doi.org/10.5194/amt-2018-235
Manuscript under review for journal Atmos. Meas. Tech.
Discussion started: 6 August 2018

Atmospheric Measurement Techniques Discussions

and in-orbit variations of GOME-2 slit function are corrected by deriving effective slit functions with a stretched preflight GOME-2 slit function and by including a resolution correction function as a pseudo absorber cross-section in the DOAS fit, respectively. Compared to the GDP 4.8 algorithm, the NO_2 columns from GDP 4.9 are higher by $\sim$1-3 $\times 10^{14}$ molec/cm^2 (up to 27%) and the NO_2 slant column noise is lower by $\sim$24%. In addition, the effect of using a new version (6.1) of the GOME-2 level 1b data has been analyzed in our NO_2 algorithm. The application of new GOME-2 level 1b data largely reduces the offset between GOME-2A and GOME-2B NO_2 columns by removing calibration artefacts in the GOME-2B irradiances (due to Xe-line contaminations in the calibration key-data). Compared to the GOME-2 NO_2 product from the QA4ECV project, the NO_2 columns from GDP 4.9 show good consistency and the NO_2 slant column noise is $\sim$14%-28% smaller, indicating a good overall quality of the improved DOAS retrieval.

The stratosphere-troposphere separation algorithm STREAM, which was designed for TROPOMI, was optimized for GOME-2 instrument. Compared to the spatial filtering method used in the GDP 4.8, STREAM provides an improved treatment of polluted and cloudy pixels by defining weighting factors for each measurement depending on polluted situation and cloudy information. For the adaption to GOME-2 measurements, the performance of STREAM is analyzed by applying it to synthetic GOME-2 data and by comparing the difference between estimated and original stratospheric fields. Applied to synthetic GOME-2 data calculated by a RTM using C-IFS model data, the estimated stratospheric NO_2 columns from STREAM show good consistency with the a priori truth. A slight overestimation by $\sim 1-2 \times 10^{14}$ molec/cm^2 is found over lower latitudes, and larger differences of up to $\sim 5 \times 10^{14}$ molec/cm^2 are found at higher latitudes. To reduce the biases over the subtropical regions in winter, an improved latitudinal correction is used in STREAM. Applied to GOME-2 measurements, the updated STREAM separates successfully the stratospheric and tropospheric contribution over polluted regions, especially in the northern hemisphere. Compared to the current method in the GDP 4.8, the use of STREAM slightly decreases the stratospheric NO_2 columns by $\sim 1 \times 10^{14}$ molec/cm^2 in general and largely reduces the overestimation over polluted areas.

To improve the calculation of NO_2 AMF, a new box-AMF LUT was generated using the latest version of the VLIDORT RTM with an increased number of reference points and vertical layers to reduce interpolation errors. The new GOME-2 surface LER climatology (Tilstra et al., 2017b) used in this study is derived with a high resolution of 1°lon×1°lat (0.25°lon×0.25°lat at coastlines) and an improved LER algorithm based on observations for 2007-2013. Daily a priori NO_2 profiles, obtained from the chemistry transport model TM5-MP, capture the short-term variability in the NO_2 fields with a resolution of 1°lon×1°lat. Cloud parameters are retrieved using a new version 3.0 of the OCRA/ROCINN algorithm. A large impact on the retrieved tropospheric NO_2 columns (more than 10%) is found over polluted areas.

The uncertainty in our GDP 4.9 NO_2 slant columns is 4.4×10^{14} molec/cm^2, calculated from the average slant column error using a statistical method described in Sect. 4.5. The uncertainty in the GOME-2 stratospheric columns is $\sim 4-5 \times 10^{14}$ molec/cm^2 for polluted conditions based on the daily synthetic GOME-2 data and $\sim 1-2 \times 10^{14}$ molec/cm^2 for monthly averages. The uncertainty in the tropospheric AMFs is estimated to be in the 10−35% range, considering the use of updated box-AMF LUT and improved surface albedo climatology, a priori NO_2 profiles, and cloud parameters, resulting in a total uncertainty in the tropospheric NO_2 columns likely in the range of 30−50% for polluted conditions.

An end-to-end validation of the improved GOME-2 GDP 4.9 dataset was performed by comparing the GOME-2 tropospheric NO_2 columns with BIRA-IASB ground-based MAXDOAS measurements. The validation was illustrated for different MAXDOAS stations (Beijing, Bujumbura, OHP, Reunion, Uccle, and Xianghe) covering urban, suburban, and background situations. Taking Xianghe station as an example, the GDP 4.9 dataset shows a similar seasonal variation in the tropospheric NO_2 columns as the MAXDOAS measurements with a relative difference of -5.8% and a correlation coefficient of 0.91, indicating a good agreement. Compared to the current operational GDP 4.8 product, the GDP 4.9 dataset is a significant improvement. Although GOME-2 measurements are still underestimating the tropospheric NO_2 columns with respect to the ground data, the absolute and relative differences with the different MAXDOAS stations are smaller, both for the original comparisons and for the comparisons with the smoothed MAXDOAS columns.

In the future, the AMF calculation will be further improved, since uncertainty in AMF is one dominating source of errors in the tropospheric NO_2 retrieval, especially over polluted areas. The surface Bidirectional Reflectance Distribution Function (BRDF) effect will be included using a direction-dependent LER climatology from GOME-2 (Tilstra, L., personal communication) to describe the angular distribution of the surface reflectance. Aerosol properties will be considered explicitly in the RTM calculation using ground-based aerosol observations from e.g. MAXDOAS instruments, Mie scattering Lidars, or sun photometers operated by the AErosol RObotic NETwork (AERONET). A priori NO_2 profiles from different global and regional models will help to analyse the effect of spatial resolution, temporal resolution, and emission on the tropospheric NO_2 retrieval for GOME-2. Furthermore, the NO_2 algorithm will be adapted to measurements from the TROPOMI instrument with a spatial resolution as high as 7×3.5 km^2.

Acknowledgements. This work is funded by the DLR-DAAD Research Fellowships 2015 (57186656) programme with reference number 91585186 and is undertaken in the framework of the EUMETSAT AC-SAF project. We acknowledge the Belgian Science Policy Office (BELSPO) supporting part of this work through the PRODEX project B-ACSAF. We thank EUMETSAT for the ground segment interfacing work and for the provision of GOME-2 level 1 products. We thank the UPAS team for the development work on the UPAS system at DLR. We are thankful to Rüdiger Lang (EUMETSAT) for providing the GOME-2 level 1b testing data, Vincent Huijnen (KNMI) for providing the C-IFS model data, Gijsbert Tilstra (KNMI) for discussions on surface albedo, and Henk Eskes (KNMI) for creating the TM5-MP a priori NO_2 profiles. We acknowledge the free use of GOME-2 NO_2 column data from QA4ECV project available at www.qa4ecv.eu. We also acknowledge the free use of the GOME-2 surface LER database created by KNMI and provided through the AC-SAF of EUMETSAT.

Atmos. Meas. Tech. Discuss., https://doi.org/10.5194/amt-2018-235
Manuscript under review for journal Atmos. Meas. Tech.
Discussion started: 6 August 2018

Atmospheric Measurement Techniques Discussions

References

Azam, F., Richter, A., Weber, M., Noë, S., and Burrows, J.: GOME-2 on MetOp-B Follow-on analysis of GOME2 in orbit degradation, Tech. rep., EUM/CO/09/4600000696/RM, Final Report, IUP University of Bremen, 2015.

Barkley, M. P., Smedt, I. D., Van Roozendael, M., Kurosu, T. P., Chance, K., Arneth, A., Hagberg, D., Guenther, A., Paulot, F., Marais, E., et al.: Top-down isoprene emissions over tropical South America inferred from SCIAMACHY and OMI formaldehyde columns, J. Geophys. Res. Atmos., 118, 6849–6868, 2013.

Beirle, S., Hörmann, C., Jöckel, P., Liu, S., Penning de Vries, M., Pozzer, A., Sihler, H., Valks, P., and Wagner, T.: The STRatospheric Estimation Algorithm from Mainz (STREAM): estimating stratospheric NO2 from nadir-viewing satellites by weighted convolution, Atmos. Meas. Tech., 9, 2753–2779, 2016.

Beirle, S., Lampel, J., Lerot, C., Sihler, H., and Wagner, T.: Parameterizing the instrumental spectral response function and its changes by a super-Gaussian and its derivatives, Atmos. Meas. Tech., 10, 581, 2017.

Boersma, K., Bucsela, E., Brinksma, E., and Gleason, J.: OMI algorithm theoretical basis document: OMI trace gas algorithms, vol. 4, edited by K. Chance, Rep. ATBD-OMI, 2, 2002.

Boersma, K., Eskes, H., and Brinksma, E.: Error analysis for tropospheric NO2 retrieval from space, J. Geophys. Res. Atmos., 109, 2004.

Boersma, K., Eskes, H., Dirksen, R., Veefkind, J., Stammes, P., Huijnen, V., Kleipool, Q., Sneep, M., Claas, J., Leitão, J., et al.: An improved tropospheric NO2 column retrieval algorithm for the Ozone Monitoring Instrument, Atmos. Meas. Tech., 4, 1905, 2011.

Boersma, K., Vinken, G., and Eskes, H.: Representativeness errors in comparing chemistry transport and chemistry climate models with satellite UV–Vis tropospheric column retrievals, Geosci. Model Dev., 9, 875, 2016.

Boersma, K., Eskes, H., Richter, A., De Smedt, I., Lorente, A., Beirle, S., Van Geffen, J., Zara, M., Peters, E., Van Roozendael, M., Wagner, T., Maasakkers, J., van der A, R., Nighttingale, J., De Rudder, A., Irie, H., Pinardi, G., Lambert, J.-C., and Compernolle: Improving algorithms and uncertainty estimates for satellite NO2 retrievals: Results from the Quality Assurance for Essential Climate Variables (QA4ECV) project, submitted, 2018.

Bovensmann, H., Burrows, J., Buchwitz, M., Frerick, J., Rozanov, V., Chance, K., and Goede, A.: SCIAMACHY: Mission objectives and measurement modes, J. Atmos. Sci., 56, 1999.

Brion, J., Chakir, A., Charbonnier, J., Daumont, D., Parisse, C., and Malicet, J.: Absorption spectra measurements for the ozone molecule in the 350–830 nm region, J. Atmos. Chem., 30, 291–299, 1998.

Bucsela, E., Krotkov, N., Celarier, E., Lamsal, L., Swartz, W., Bhartia, P., Boersma, K., Veefkind, J., Gleason, J., and Pickering, K.: A new stratospheric and tropospheric NO2 retrieval algorithm for nadir-viewing satellite instruments: applications to OMI, Atmos. Meas. Tech., 6, 2607, 2013.

Burrows, J. P., Weber, M., Buchwitz, M., Rozanov, V., Ladstätter-Weißenmayer, A., Richter, A., DeBeek, R., Hoogen, R., Bramstedt, K., Eichmann, K.-U., et al.: The global ozone monitoring experiment (GOME): Mission concept and first scientific results, J. Atmos. Sci., 56, 151–175, 1999.

Callies, J., Corpaccioli, E., Eisinger, M., Hahne, A., and Lefebvre, A.: GOME-2-Metop's second-generation sensor for operational ozone monitoring, ESA bulletin, 102, 28–36, 2000.

Celarier, E., Brinksma, E., Gleason, J., Veefkind, J., Cede, A., Herman, J., Ionov, D., Goutail, F., Pommereau, J.-P., Lambert, J.-C., et al.: Validation of Ozone Monitoring Instrument nitrogen dioxide columns, J. Geophys. Res. Atmos., 113, 2008.

Chance, K. and Kurucz, R.: An improved high-resolution solar reference spectrum for earth's atmosphere measurements in the ultraviolet, visible, and near infrared, J. Quant. Spectrosc. Radiat. Transf., 111, 1289–1295, 2010.

Chen, D., Zhou, B., Beirle, S., Chen, L., and Wagner, T.: Tropospheric NO2 column densities deduced from zenith-sky DOAS measurements in Shanghai, China, and their application to satellite validation, Atmos. Chem. Phys., 9, 3641–3662, 2009.

Clémer, K., Van Roozendael, M., Fayt, C., Hendrick, F., Hermans, C., Pinardi, G., Spurr, R., Wang, P., and De Mazière, M.: Multiple wavelength retrieval of tropospheric aerosol optical properties from MAXDOAS measurements in Beijing, Atmos. Meas. Tech., 3, 863, 2010.

Danckaert, T., Fayt, C., Van Roozendael, M., De Smedt, I., Letocart, V., Merlaud, A., and Pinardi, G.: QDOAS software user manual 2.109, IASB/BIRA, Uccle, Belgium, 2015.

De Smedt, I., Van Roozendael, M., Stavrakou, T., Müller, J., Lerot, C., Theys, N., Valks, P., Hao, N., and Van Der A, R.: Improved retrieval of global tropospheric formaldehyde columns from GOME-2/MetOp-A addressing noise reduction and instrumental degradation issues, Atmos. Meas. Tech., 5, 2933–2949, 2012.

Dikty, S., Richter, A., Weber, M., Noël, S., Bovensmann, H., Wittrock, F., and Burrows, J.: GOME-2 on MetOp-A Support for Analysis of GOME-2 In-Orbit Degradation and Impacts on Level 2 Data Products–Final Report, Tech. rep., ITT 09/10000262, IUP University of Bremen, 2011.

Ding, J., Miyazaki, K., Mijling, B., Kurokawa, J.-i., Cho, S., Janssens-Maenhout, G., Zhang, Q., Liu, F., Levelt, P. F., et al.: Intercomparison of NOx emission inventories over East Asia, Atmos. Chem. Phys., 17, 10 125, 2017.

Doicu, A., Trautmann, T., and Schreier, F.: Numerical regularization for atmospheric inverse problems, Springer Science & Business Media, 2010.

Drosoglou, T., Bais, A. F., Zyrichidou, I., Kouremeti, N., Poupkou, A., Liora, N., Giannaros, C., Koukouli, M. E., Balis, D., and Melas, D.: Comparisons of ground-based tropospheric NO2 MAX-DOAS measurements to satellite observations with the aid of an air quality model over the Thessaloniki area, Greece, Atmos. Chem. Phys., 17, 5829–5849, 2017.

Drosoglou, T., Koukouli, M. E., Kouremeti, N., Bais, A. F., Zyrichidou, I., Balis, D., Xu, J., Li, A., et al.: MAX-DOAS NO2 observations over Guangzhou, China; ground-based and satellite comparisons, Atmos. Meas. Tech., 11, 2239–2255, 2018.

Eskes, H. and Boersma, K.: Averaging kernels for DOAS total-column satellite retrievals, Atmos. Chem. Phys., 3, 1285–1291, 2003.

EUMETSAT: GOME-2 Products Guide, Tech. rep., Ref.: EUM/OPSEPS/MAN/07/0445, Issue: v2D, 2009.

EUMETSAT: GOME-2/Metop-A Level 1B Product Validation Report No. 5: Status at Reprocessing, Tech. rep., EUM/OPS/EPS/REP/09/0619, v1F, 2012.

EUMETSAT: GOME-2 Newsletter Archive, Tech. rep., EUM/OPS-EPS/TEN/09/0552, 2015.

European Commission: The EU Environmental Implementation Review: Common challenges and how to combine efforts to deliver better results, Tech. rep., Ref.: SWD(2017)33-60 fina, 2017.

Gielen, C., Hendrick, F., Pinardi, G., De Smedt, I., Fayt, C., Hermans, C., Stavrakou, T., Bauwens, M., Müller, J.-F., Ndenzako, E., Nzohabonayo, P., Akimana, R., Niyonzima, S., Van Roozendael, M., and De Mazière, M.: Characterisation of Central-African aerosol and trace-gas emissions based on MAX-DOAS measurements and model simulations over Bujumbura, Burundi., Atmospheric Chemistry and Physics Discussions, pp. 1–41, 2017.

Granier, C., Bessagnet, B., Bond, T., D'Angiola, A., van Der Gon, H. D., Frost, G. J., Heil, A., Kaiser, J. W., Kinne, S., Klimont, Z., et al.: Evolution of anthropogenic and biomass burning emissions of air pollutants at global and regional scales during the 1980–2010 period, Climatic Change, 109, 163, 2011.

Gu, D., Wang, Y., Smeltzer, C., and Boersma, K. F.: Anthropogenic emissions of NOx over China: Reconciling the difference of inverse modeling results using GOME-2 and OMI measurements, J. Geophys. Res. Atmos., 119, 7732–7740, 2014.

Hassinen, S., Balis, D., Bauer, H., Begoin, M., Delcloo, A., Eleftheratos, K., Garcia, S. G., Granville, J., Grossi, M., Hao, N., et al.: Overview of the O3M SAF GOME-2 operational atmospheric composition and UV radiation data products and data availability, Atmos. Meas. Tech., 9, 383, 2016.

Heckel, A., Richter, A., Tarsu, T., Wittrock, F., Hak, C., Pundt, I., Junkermann, W., and Burrows, J.: MAX-DOAS measurements of formaldehyde in the Po-Valley, Atmos. Chem. Phys., 5, 909–918, 2005.

Heckel, A., Kim, S.-W., Frost, G., Richter, A., Trainer, M., and Burrows, J.: Influence of low spatial resolution a priori data on tropospheric NO2 satellite retrievals, Atmos. Meas. Tech., 4, 1805, 2011.

Hendrick, F., Müller, J.-F., Clémer, K., Wang, P., Mazière, M. D., Fayt, C., Gielen, C., Hermans, C., Ma, J., Pinardi, G., et al.: Four years of ground-based MAX-DOAS observations of HONO and NO2 in the Beijing area, Atmos. Chem. Phys., 14, 765–781, 2014.

Hilboll, A., Richter, A., and Burrows, J.: Long-term changes of tropospheric NO2 over megacities derived from multiple satellite instruments, Atmos. Chem. Phys., 13, 4145–4169, 2013.

Hilboll, A., Richter, A., and Burrows, J. P.: NO2 pollution over India observed from space–The impact of rapid economic growth, and a recent decline, Atmospheric Chemistry and Physics Discussions, 2017.

Hönninger, G., Friedeburg, C. v., and Platt, U.: Multi axis differential optical absorption spectroscopy (MAX-DOAS), Atmos. Chem. Phys., 4, 231–254, 2004.

Horowitz, L. W., Walters, S., Mauzerall, D. L., Emmons, L. K., Rasch, P. J., Granier, C., Tie, X., Lamarque, J.-F., Schultz, M. G., Tyndall, G. S., et al.: A global simulation of tropospheric ozone and related tracers: Description and evaluation of MOZART, version 2, J. Geophys. Res. Atmos., 108, 2003.

Huijnen, V., Williams, J., Weele, M. v., Noije, T. v., Krol, M., Dentener, F., Segers, A., Houweling, S., Peters, W., Laat, J. d., et al.: The global chemistry transport model TM5: description and evaluation of the tropospheric chemistry version 3.0, Geoscientific Model Development, 3, 445–473, 2010.

Huijnen, V., Flemming, J., Chabrillat, S., Errera, Q., Christophe, Y., Blechschmidt, A.-M., Richter, A., and Eskes, H.: C-IFS-CB05-BASCOE: stratospheric chemistry in the Integrated Forecasting System of ECMWF, Geosci. Model Dev., 9, 3071–3091, 2016.

Ingmann, P., Veihelmann, B., Langen, J., Lamarre, D., Stark, H., and Courrèges-Lacoste, G. B.: Requirements for the GMES Atmosphere Service and ESA's implementation concept: Sentinels-4/-5 and-5p, Remote sensing of environment, 120, 58–69, 2012.

Irie, H., Takashima, H., Kanaya, Y., Boersma, K., Gast, L., Wittrock, F., Brunner, D., Zhou, Y., and Roozendael, M. V.: Eight-component retrievals from ground-based MAX-DOAS observations, Atmos. Meas. Tech., 4, 1027–1044, 2011.

Irie, H., Boersma, K., Kanaya, Y., Takashima, H., Pan, X., and Wang, Z.: Quantitative bias estimates for tropospheric NO2 columns retrieved from SCIAMACHY, OMI, and GOME-2 using a common standard for East Asia, Atmos. Meas. Tech., 5, 2403–2411, 2012.

Kanaya, Y., Irie, H., Takashima, H., Iwabuchi, H., Akimoto, H., Sudo, K., Gu, M., Chong, J., Kim, Y., Lee, H., et al.: Long-term MAX-DOAS network observations of NO2 in Russia and Asia (MADRAS) during the period 2007–2012: instrumentation, elucidation of climatology, and comparisons with OMI satellite observations and global model simulations., Atmospheric Chemistry & Physics, 14, 2014.

Kim, J.: GEMS (Geostationary Environment Monitoring Spectrometer) onboard the GeoKOMPSAT to monitor air quality in high temporal and spatial resolution over Asia-Pacific Region, in: EGU General Assembly Conference Abstracts, vol. 14, p. 4051, 2012.

Kleipool, Q., Dobber, M., de Haan, J., and Levelt, P.: Earth surface reflectance climatology from 3 years of OMI data, J. Geophys. Res. Atmos., 113, 2008.

Kramer, L. J., Leigh, R. J., Remedios, J. J., and Monks, P. S.: Comparison of OMI and ground-based in situ and MAX-DOAS measurements of tropospheric nitrogen dioxide in an urban area, J. Geophys. Res. Atmos., 113, 2008.

Lambert, J., Granville, J., Van Roozendael, M., Sarkissian, A., Goutail, F., Müller, J., Pommereau, J., and Russell III, J.: A climatology of NO2 profile for improved air mass factors for ground-based vertical column measurements, in: Proceedings of the 5th European Symposium Strat. Ozone, Saint Jean de Luz, p. 703, 1999.

Lampel, J., Pöhler, D., Tschritter, J., Frieß, U., and Platt, U.: On the relative absorption strengths of water vapour in the blue wavelength range, Atmos. Meas. Tech., 8, 4329–4346, 2015.

Leitão, J., Richter, A., Vrekoussis, M., Kokhanovsky, A., Zhang, Q., Beekmann, M., and Burrows, J.: On the improvement of NO2 satellite retrievals–aerosol impact on the airmass factors, Atmos. Meas. Tech., 3, 475–493, 2010.

Levelt, P., Van den Oord, G., Dobber, M., Malkki, A., Visser, H., de Vries, J., Stammes, P., Lundell, J., and Saari, H.: The Ozone Monitoring Instrument, IEEE T. Geosci. Remote Sens., 44, 1093–1101, 2006.

Lin, J., Martin, R., Boersma, K., Sneep, M., Stammes, P., Spurr, R., Wang, P., Van Roozendael, M., Clémer, K., and Irie, H.: Retrieving tropospheric nitrogen dioxide from the Ozone Monitoring Instrument: effects of aerosols, surface reflectance anisotropy, and vertical profile of nitrogen dioxide, Atmos. Chem. Phys., 14, 1441–1461, 2014.

Lin, J., Liu, M., Xin, J., Boersma, K., Spurr, R., Martin, R., and Zhang, Q.: Influence of aerosols and surface reflectance on satellite NO2 retrieval: seasonal and spatial characteristics and implications for NOx emission constraints, Atmos. Chem. Phys., 15, 11 217, 2015.

Liu, F., Beirle, S., Zhang, Q., Zheng, B., Tong, D., He, K., et al.: NOx emission trends over Chinese cities estimated from OMI observations during 2005 to 2015, Atmos. Chem. Phys., 17, 9261–9275, 2017.

Lorente, A., Boersma, K. F., Yu, H., Dörner, S., Hilboll, A., Richter, A., Liu, M., Lamsal, L. N., Barkley, M., De Smedt, I., et al.: Structural uncertainty in air mass factor calculation for NO2 and HCHO satellite retrievals, Atmos. Meas. Tech., 10, 759, 2017.

Loyola, D., Thomas, W., Livschitz, Y., Ruppert, T., Albert, P., and Hollmann, R.: Cloud properties derived from GOME/ERS-2 backscatter data for trace gas retrieval, IEEE Trans. Geosci. Remote Sens., 45, 2747–2758, 2007.

Loyola, D., Koukouli, M., Valks, P., Balis, D., Hao, N., Van Roozendael, M., Spurr, R., Zimmer, W., Kiemle, S., Lerot, C., et al.: The GOME-2 total column ozone product: Retrieval algorithm and ground-based validation, J. Geophys. Res. Atmos., 116, 2011.

Loyola, D. G., Pedergnana, M., and García, S. G.: Smart sampling and incremental function learning for very large high dimensional data, Neural Networks, 78, 75–87, 2016.

Loyola, D. G., García, S. G., Lutz, R., Argyrouli, A., Romahn, F., Spurr, R. J., Pedergnana, M., Doicu, A., García, V. M., and Schüssler, O.: The operational cloud retrieval algorithms from TROPOMI on board Sentinel-5 Precursor, Atmos. Meas. Tech., 11, 409, 2018.

Lutz, R., Loyola, D., Gimeno García, S., and Romahn, F.: OCRA radiometric cloud fractions for GOME-2 on MetOp-A/B, Atmos. Meas. Tech., 9, 2357–2379, 2016.

Ma, J., Beirle, S., Jin, J., Shaiganfar, R., Yan, P., and Wagner, T.: Tropospheric NO2 vertical column densities over Beijing: results of the first three years of ground-based MAX-DOAS measurements (2008–2011) and satellite validation, Atmos. Chem. Phys., 13, 1547–1567, 2013.

Mijling, B., Ding, J., Koukouli, M. E., Liu, F., Li, Q., Mao, H., Theys, N., et al.: Cleaning up the air: effectiveness of air quality policy for SO2 and NOx emissions in China, Atmos. Chem. Phys., 17, 1775–1789, 2017.

Miyazaki, K., Eskes, H., Sudo, K., Boersma, K. F., Bowman, K., and Kanaya, Y.: Decadal changes in global surface NOx emissions from multi-constituent satellite data assimilation, Atmos. Chem. Phys, 17, 807–837, 2017.

Müller, J.-P., Kharbouche, S., Gobron, N., Scanlon, T., Govaerts, Y., Danne, O., Schultz, J., Lattanzio, A., Peters, E., De Smedt, I., Beirle, S., Lorente, A., Coheur, P., George, M., Wagner, T., Hilboll, A., Richter, A., Van Roozendael, M., and Boersma, K.: Recommendations (scientific) on best practices for retrievals for Land and Atmosphere ECVs, Tech. rep., Deliverable 4.2 - version 1.0, 2016.

Munro, R., Lang, R., Klaes, D., Poli, G., Retscher, C., Lindstrot, R., Huckle, R., Lacan, A., Grzegorski, M., Holdak, A., et al.: The GOME-2 instrument on the Metop series of satellites: instrument design, calibration, and level 1 data processing–an overview, Atmos. Meas. Tech., 9, 1279–1301, 2016.

Nüß, H., Richter, A., Valks, P., and Burrows, J.: Improvement of the NO2 total column retrieval for GOME-2, O3M SAF Visiting Scientist Activity, Final Report, IUP University of Bremen, 2006.

Olivier, J. G., Bouwman, A., Berdowski, J., Veldt, C., Bloos, J., Visschedijk, A., Zandveld, P., Haverlag, J., et al.: Description of EDGAR Version 2.0: A set of global emission inventories of greenhouse gases and ozone-depleting substances for all anthropogenic and most natural sources on a per country basis and on 1 degree x 1 degree grid, 1996.

Ortega, I., Koenig, T., Sinreich, R., Thomson, D., and Volkamer, R.: The CU 2-D-MAX-DOAS instrument–Part 1: Retrieval of 3-D distributions of NO2 and azimuth-dependent OVOC ratios, Atmos. Meas. Tech., 8, 2371, 2015.

Penning de Vries, M., Beirle, S., Hörmann, C., Kaiser, J., Stammes, P., Tilstra, L., and Wagner, T.: A global aerosol classification algorithm incorporating multiple satellite data sets of aerosol and trace gas abundances, Atmos. Chem. Phys., 15, 10 597–10 618, 2015.

Peters, E., Wittrock, F., Richter, A., Alvarado, L., Rozanov, V., and Burrows, J.: Liquid water absorption and scattering effects in DOAS retrievals over oceans, Atmos. Meas. Tech., 7, 4203–4221, 2014.

Pinardi, G., Van Roozendael, M., Lambert, J., Granville, J., Hendrick, F., Tack, F., Yu, H., Cede, A., Kanaya, Y., Irie, I., et al.: GOME-2 total and tropospheric NO2 validation based on zenith-sky, direct-sun and multi-axis DOAS network observations, in: Proc. of the 2014 EUMETSAT Meteorological Satellite Conference, Geneva, Swizerland, EUMETSAT, 2014.

Pinardi, G., Lambert, J.-C., Granville, J., Yu, H., De Smedt, I., van Roozendael, M., and Valks, P.: O3M-SAF validation report, Tech. rep., SAF/O3M/IASB/VR/NO2/TN-IASB-GOME2-O3MSAF-NO2-2015, Issue 1/1, 2015.

Platt, U. and Stutz, J.: Differential Optical Absorption Spectroscopy, Springer, 2008.

Pope, R. M. and Fry, E. S.: Absorption spectrum (380–700 nm) of pure water. II. Integrating cavity measurements, Appl. Opt., 36, 8710–8723, 1997.

Richter, A. and verification team, S.-P.: S5P/TROPOMI Science Verification Report, Tech. rep., S5P-IUP-L2-ScVR-RP issue 2.1, 2015.

Richter, A., Burrows, J. P., Nüß, H., Granier, C., and Niemeier, U.: Increase in tropospheric nitrogen dioxide over China observed from space, Nature, 437, 129, 2005.

Richter, A., Begoin, M., Hilboll, A., and Burrows, J.: An improved NO2 retrieval for the GOME-2 satellite instrument, Atmos. Meas. Tech., 4, 1147–1159, 2011.

Rothman, L., Gordon, I., Barber, R., Dothe, H., Gamache, R., Goldman, A., Perevalov, V., Tashkun, S., and Tennyson, J.: HITEMP, the high-temperature molecular spectroscopic database, Journal of Quantitative Spectroscopy and Radiative Transfer, 111, 2139–2150, 2010.

Safieddine, S., Clerbaux, C., George, M., Hadji-Lazaro, J., Hurtmans, D., Coheur, P.-F., Wespes, C., Loyola, D., Valks, P., and Hao, N.: Tropospheric ozone and nitrogen dioxide measurements in urban and rural regions as seen by IASI and GOME-2, J. Geophys. Res. Atmos., 118, 2013.

Seinfeld, J. H., Pandis, S., and Noone, K.: Atmospheric chemistry and physics: from air pollution to climate change, 1998.

Solomon, S.: Stratospheric ozone depletion: A review of concepts and history, Rev. Geophys., 37, 275–316, 1999.

Spurr, R., Kurosu, T., and Chance, K.: A linearized discrete ordinate radiative transfer model for atmospheric remote-sensing retrieval, J. Quant. Spectrosc. Radiat. Transf., 68, 689–735, 2001.

Spurr, R. J.: VLIDORT: A linearized pseudo-spherical vector discrete ordinate radiative transfer code for forward model and retrieval studies in multilayer multiple scattering media, Journal of Quantitative Spectroscopy and Radiative Transfer, 102, 316–342, 2006.

Thalman, R. and Volkamer, R.: Temperature dependent absorption cross-sections of O 2–O 2 collision pairs between 340 and 630 nm and at atmospherically relevant pressure, Phys. Chem. Chem. Phys., 15, 15 371–15 381, 2013.

Tikhonov, A. and Arsenin, V.: Solutions of ill-posed problems Wiley, New York, 258, 1977.

Tilstra, L., Tuinder, O., and Stammes, P.: GOME-2 surface LER product - Algorithm Theoretical Basis Document, Tech. rep., KNMI Report O3MSAF/KNMI/ATBD/003, Issue 2.2, 2017a.

Tilstra, L., Wang, P., and Stammes, P.: Surface reflectivity climatologies from UV to NIR determined from Earth observations by GOME-2 and SCIAMACHY, J. Geophys. Res. Atmos., 122, 4084–4111, 2017b.

Valks, P., Pinardi, G., Richter, A., Lambert, J.-C., Hao, N., Loyola, D., Van Roozendael, M., and Emmadi, S.: Operational total and tropospheric NO2 column retrieval for GOME-2, Atmos. Meas. Tech., 4, 1491, 2011.

Valks, P., Loyola, D., Hao, N., Hedelt, P., Slijkhuis, S., Grossi, M., Begoin, M., Gimeno Garcia, S., and Lutz, R.: Algorithm Theoretical Basis Document for GOME-2 Total Column Products of Ozone, NO2, BrO, SO2, H2O, HCHO and Cloud Properties (GDP 4.8 for AC SAF OTO and NTO), Tech. rep., SAF/AC/DLR/ATBD/01, Iss./Rev.: 3/A/2, 2017.

van Geffen, J., Boersma, K., Van Roozendael, M., Hendrick, F., Mahieu, E., De Smedt, I., Sneep, M., and Veefkind, J.: Improved spectral fitting of nitrogen dioxide from OMI in the 405–465 nm window, Atmos. Meas. Tech., 8, 1685–1699, 2015.

van Geffen, J., Boersma, K., Eskes, H., Maasakkers, J., and Veefkind, J.: TROPOMI ATBD of the total and tropospheric NO2 data products, Tech. rep., S5P-KNMI-L2-0005-RP issue 1.0.0. KNMI, De Bilt, the Netherlands, 2016.

Vandaele, A. C., Hermans, C., Fally, S., Carleer, M., Colin, R., Merienne, M.-F., Jenouvrier, A., and Coquart, B.: High-resolution Fourier transform measurement of the NO2 visible and near-infrared absorption cross sections: Temperature and pressure effects, J. Geophys. Res. Atmos., 107, 2002.

Veefkind, J., Aben, I., McMullan, K., Förster, H., De Vries, J., Otter, G., Claas, J., Eskes, H., De Haan, J., Kleipool, Q., et al.: TROPOMI on the ESA Sentinel-5 Precursor: A GMES mission for global observations of the atmospheric composition for climate, air quality and ozone layer applications, Remote Sens. Environ., 120, 70–83, 2012.

Vlemmix, T., Hendrick, F., Pinardi, G., De Smedt, I., Fayt, C., Hermans, C., Piters, A., Wang, P., Levelt, P., and Van Roozendael, M.: MAX-DOAS observations of aerosols, formaldehyde and nitrogen dioxide in the Beijing area: comparison of two profile retrieval approaches, Atmos. Meas. Tech., 8, 941, 2015.

Vountas, M., Richter, A., Wittrock, F., and Burrows, J.: Inelastic scattering in ocean water and its impact on trace gas retrievals from satellite data, Atmos. Chem. Phys., 3, 1365–1375, 2003.

Vrekoussis, M., Wittrock, F., Richter, A., and Burrows, J.: GOME-2 observations of oxygenated VOCs: what can we learn from the ratio glyoxal to formaldehyde on a global scale?, Atmos. Chem. Phys., 10, 10 145–10 160, 2010.

Wagner, T., Dix, B. v., Friedeburg, C. v., Frieß, U., Sanghavi, S., Sinreich, R., and Platt, U.: MAX-DOAS O4 measurements: A new technique to derive information on atmospheric aerosols—Principles and information content, J. Geophys. Res. Atmos., 109, 2004.

Wagner, T., Beirle, S., Brauers, T., Deutschmann, T., Frieß, U., Hak, C., Halla, J., Heue, K., Junkermann, W., Li, X., et al.: Inversion of tropospheric profiles of aerosol extinction and HCHO and NO2 mixing ratios from MAX-DOAS observations in Milano during the summer of 2003 and comparison with independent data sets, Atmos. Meas. Tech., 4, 2685–2715, 2011.

Wang, Y., Beirle, S., Lampel, J., Koukouli, M., De Smedt, I., Theys, N., Ang, L., Wu, D., Xie, P., Liu, C., et al.: Validation of OMI, GOME-2A and GOME-2B tropospheric NO2, SO2 and HCHO products using MAX-DOAS observations from 2011 to 2014 in Wuxi, China: investigation of the effects of priori profiles and aerosols on the satellite products, Atmos. Chem. Phys., 17, 5007, 2017.

Williams, J. E., Boersma, K. F., Le Sager, P., and Verstraeten, W. W.: The high-resolution version of TM5-MP for optimized satellite retrievals: description and validation, Geoscientific Model Development, 10, 721, 2017.

Wittrock, F., Oetjen, H., Richter, A., Fietkau, S., Medeke, T., Rozanov, A., and Burrows, J.: MAX-DOAS measurements of atmospheric trace gases in Ny-Ålesund-Radiative transfer studies and their application, Atmos. Chem. Phys., 4, 955–966, 2004.

Wu, F., Xie, P., Li, A., Chan, K., Hartl, A., Wang, Y., Si, F., Zeng, Y., Qin, M., Xu, J., et al.: Observations of SO2 and NO2 by mobile DOAS in the Guangzhou eastern area during the Asian Games 2010, Atmospheric Measurement Techniques, 6, 2277–2292, 2013.

Zara, M., Boersma, K. F., De Smedt, I., Richter, A., Peters, E., Van Geffen, J. H. G. M., Beirle, S., Wagner, T., Van Roozendael, M., Marchenko, S., Lamsal, L. N., and Eskes, H. J.: Improved slant column density retrieval of nitrogen dioxide and formaldehyde for OMI and GOME-2A from QA4ECV: intercomparison, uncertainty characterization, and trends, Atmospheric Measurement Techniques Discussions, 2018, 1–47, 2018.

Zien, A., Richter, A., Hilboll, A., Blechschmidt, A.-M., and Burrows, J.: Systematic analysis of tropospheric NO 2 long-range transport events detected in GOME-2 satellite data., Atmospheric Chemistry & Physics, 14, 2014.

Zoogman, P., Liu, X., Suleiman, R., Pennington, W., Flittner, D., Al-Saadi, J., Hilton, B., Nicks, D., Newchurch, M., Carr, J., et al.: Tropospheric emissions: Monitoring of pollution (TEMPO), Journal of Quantitative Spectroscopy and Radiative Transfer, 186, 17–39, 2017.